

Fluorescence Microscopy of Nicotinic  
Acetylcholine Receptors

Thesis by  
Crystal N. Dilworth

In Partial Fulfillment of the Requirements for the degree  
of  
Doctor of Philosophy



CALIFORNIA INSTITUTE OF TECHNOLOGY  
Pasadena, California  
2014  
(Defended Nov. 21<sup>st</sup> 2013)



## ACKNOWLEDGEMENTS

*To the many people who contributed to the creation of this thesis,*

*Thank you. Thank you for your love, support, compassion, and understanding. So many of you were there to encourage me along this path, and without you I might have lost my way. It is said that “it takes a village to raise a child”, and it truly has taken a whole community of caring people to make this thesis possible. All of you, possibly unknowingly, were instrumental in this achievement.*

*Thank you for helping me to become myself.*

## ABSTRACT

Neuronal nicotinic acetylcholine receptors (nAChRs) are pentameric ligand gated ion channels abundantly expressed in the central nervous system. Changes in the assembly and trafficking of nAChRs are pertinent to disease states including nicotine dependence, autosomal dominant nocturnal frontal lobe epilepsy (ADNFLE) and Parkinson's disease (PD). Here we investigate the application of high resolution fluorescence techniques for the study of nAChR assembly and trafficking. We also describe the construction and validation of a fluorescent  $\alpha 5$  subunit and subsequent experiments to elucidate the cellular mechanisms through which  $\alpha 5$  subunits are expressed, assembled into mature receptors, and trafficked to the cell surface. The effects of a known single nucleotide polymorphism, D398N, in the intracellular loop of  $\alpha 5$  are also examined

Additionally, this report describes the development of a combined total internal reflection fluorescence (TIRF) and lifetime imaging (FLIM) technique and the first application of this methodology for elucidation of stoichiometric composition of nAChRs. Many distinct subunit combinations can form functional receptors. Receptor composition and stoichiometry confers unique biophysical and pharmacological properties to each receptor sub-type. Understanding the nature of assembly and expression of each receptor subtype yields important information about the molecular processes that may underlie the mechanisms through which nAChR contribute to disease and addiction states.

## TABLE OF CONTENTS

Acknowledgements .....	iii
Abstract.....	iv
Table of Contents .....	v
Introduction .....	1
Chapter I: Construction of a Fluorescent $\alpha 5$ Subunit .....	4
Chapter II: Investigation into miR-346 Regulation of the nAChR $\alpha 5$ Subunit .....	15
Chapter III: Expression of $\alpha 5$ -mEGFP in Mouse Cortical Neurons .....	22
Chapter IV: Determination of nAChR stoichiometry using NFRET .....	31
Chapter V: TIRF-FLIM-FRET: Engineering a Technique for High Resolution Detection of nAChR of nAChR Composition and Stoichiometry.....	43
Chapter IV: Conclusions .....	57
Appendix i: Plasmid maps.....	61
PCR Protocols .....	62
Appendix ii: Transfection Protocols .....	63
N2a Cells for Fluorescence Imaging (Expressfect).....	63
N2a Cells for Differentiation and HEK293-T (Lipofectamine 2000)....	64
Neuronal Transfection Non-optimized .....	65
Neuronal Transfection Optimized.....	66
Maintenance of Neuronal Cultures .....	67
Imaging Settings .....	69
Appendix iii: Image work-up for NFRET Experiments.....	70
Statistical Analysis: t-test $\alpha 4$ vs. $\alpha 4\beta 2$ Total NFRET Pixels.....	72
Statistical Analysis: t-test $\alpha 5\alpha 4$ vs. $\alpha 5\alpha 4\beta 2$ Total NFRET Pixels .....	73
Statistical Analysis: t-test $\alpha 5\alpha 4$ vs. $\alpha 5\alpha 4\beta 2$ Mean Cell Values .....	74
Bibliography .....	75

## *Introduction*

Nicotinic Acetylcholine Receptors (nAChRs) are ligand gated ion channels found in both the peripheral and central nervous systems. These receptors can be activated by nicotine as well as their native ligand acetylcholine and have been associated with several health-related phenomena. Nicotine is the major addictive component of tobacco, and chronic tobacco use (smoking) has been implicated in many types of cancer as well as heart disease. Other related phenomena include an inverse correlation between smoking and Parkinson's disease and the observation that patients with autosomal dominant nocturnal frontal lobe epilepsy (ADNFLE) who smoke have fewer seizures [1].

Nicotinic acetylcholine receptors belong to the Cys-loop family of ionotropic receptors. Individual subunits consist of an extracellular domain (ECD), four  $\alpha$ -helical transmembrane domains, and an intracellular loop between the M3 and M4 transmembrane domains. Agonists such as acetylcholine and nicotine bind to the ECD; as a result, the pore opens and cations flow according to their electrochemical gradient.

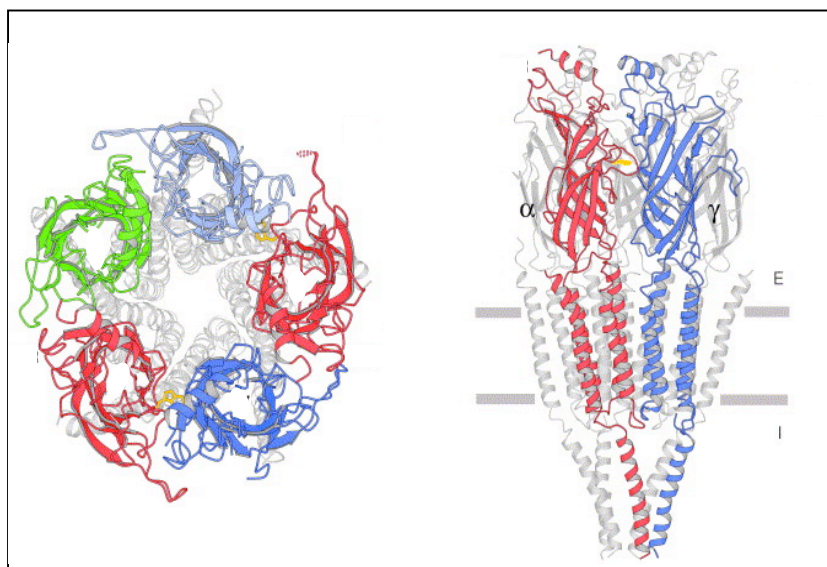


Figure 1 [2]

A. View of an assembled nAChR from the extracellular surface. Individual subunits are indicated by shading:  $\alpha 4$  and  $\beta 2$ . The **auxiliary position** can be occupied by  $\alpha 5$ .

B. Side view of the receptor. E and I designate extracellular and intracellular regions respectively. The I regions vary markedly in size and sequence among subunits, and in this view are only partially resolved.

nAChRs found in muscle are composed of two  $\alpha$  and one  $\beta$ ,  $\gamma$  (or  $\epsilon$ ) and  $\delta$  subunits [2-3]. Neuronal nAChRs are composed of  $\alpha 2$ - $\alpha 11$  and  $\beta 2$ - $\beta 4$  subunits and assemble in  $\alpha$  and  $\beta$  or  $\alpha$  only pentamers. The neuronal  $\alpha 4\beta 2$  receptor subtype is one of the two most abundant nAChRs in the central nervous system (CNS). Two  $\alpha 4\beta 2$  pentameric stoichiometries are reported:  $(\alpha 4)_3(\beta 2)_2$  and  $(\alpha 4)_2(\beta 2)_3$  [4-5]. The latter stoichiometry displays a higher sensitivity to nicotine than most other neuronal nAChRs. The subunit stoichiometry of nAChRs is important in determining its pharmacology, stability, and subcellular location. Perturbations to these properties contribute to the development of disease or dependence states. ADNFLE is a very rare monogenic disease of  $\alpha 4\beta 2$  nAChRs. The study of ADNFLE has yielded important information about nAChR stoichiometry. Point mutations associated with ADNFLE shift  $\alpha 4\beta 2$  stoichiometry to  $(\alpha 4)_3(\beta 2)_2$  [6]. This apparently affects the trafficking and pharmacology of the receptor by shifting localization to the plasma membrane (PM) and decreasing sensitivity to ACh. Nicotine use leads to reduced seizures in ADNFLE patients [1]. We know that in mammalian cells nicotine acts as a pharmacological chaperone to overcome the point mutation bias and shift stoichiometry towards  $(\alpha 4)_2(\beta 2)_3$ . Thus, ADNFLE provides a relatively simple model of how changes in  $\alpha 4\beta 2$  stoichiometry and trafficking contribute to disease [6].

Nicotine dependence is more complex than ADNFLE, although selective upregulation of  $(\alpha 4)_2(\beta 2)_3$  receptors is certainly involved. Several brain regions express  $\alpha 4$ ,  $\alpha 5$  and  $\beta 2$  subunits and assemble  $\alpha 4\beta 2\alpha 5$  receptors including the substantia nigra pars compacta, subthalamic nucleus, medial habenula, prefrontal cortex, and hippocampus [7]. Receptors containing  $\alpha 5$  also play a part in nicotine self-administration and nicotine withdrawal [8-9]. These receptors are also important for dopamine release and attention tasks [7, 10-11].

The  $\alpha 5\alpha 4\beta 2$  receptors are more permeable to  $\text{Ca}^{2+}$  than  $\alpha 4\beta 2$  receptors and have a higher sensitivity to nicotine [12]. Relative to  $(\alpha 4)_3(\beta 2)_2$ , the  $\alpha 5\alpha 4\beta 2$  receptor exhibits a higher sensitivity to acetylcholine (ACh), has increased  $\text{Ca}^{2+}$  permeability and may be resistant to upregulation by nicotine [13-14]. The  $\alpha 5$  subunit does not participate in functional agonist binding sites, and it may serve as an auxiliary subunit that modulates nAChR function when coassembled with other  $\alpha$  and  $\beta$  subunit isoforms (see figure 1).

nAChRs containing the  $\alpha 5$  subunit are especially interesting because genome wide association studies and candidate gene studies have identified polymorphisms in the  $\alpha 5$  gene that are linked to an increased risk for nicotine dependence, lung cancer, and/or alcohol addiction [15-17]. We have chosen to examine the only known coding-region polymorphism. The single nucleotide polymorphism (SNP), rs16969968, encodes an aspartic acid to asparagine mutation at position 398 in the flexible, intracellular loop that connects two transmembrane domains (the M3-M4 loop) of the human  $\alpha 5$  protein. This mutation,  $\alpha 5\text{D}398\text{N}$ , is of interest because of its association with increased risk for nicotine dependence [18]. It was hypothesized that the M3-M4 loop localization of the D398N mutation may contribute to changes in intracellular trafficking or localization of the mutant protein. Live-cell high resolution fluorescence microscopy techniques have been used to study changes to  $\alpha 4\beta 2$  receptor stoichiometry, trafficking and pharmacology. We proposed to use similar techniques to examine behavior of this receptor after inclusion of an  $\alpha 5$  or  $\alpha 5\text{D}398\text{N}$  subunit.

## *Chapter One*

### *Construction of a Fluorescent $\alpha 5$ Subunit*

The significance of the  $\alpha 5$  containing nAChR receptor ( $\alpha 5^*$  receptor) has been a challenging question for researchers since its characterization by Role et al. in 1996 [19]. Elucidation of the unique contribution of the  $\alpha 5$  subunit is complicated by several factors including the lack of  $\alpha 5$  specific pharmacological agents. As an accessory subunit,  $\alpha 5$  does not participate in ligand binding, making it difficult to selectively activate or block  $\alpha 5^*$  receptors. This challenge, combined with the similarity in  $EC_{50}$  and dose response to agonist of  $\alpha 5^*$  receptors to its parent receptors  $\alpha 4\beta 2$  or  $\alpha 3\beta 4$ , and the lack of a reliably  $\alpha 5$ -specific antibody, increases the difficulty in isolating a pure population of  $\alpha 5^*$  receptors for detailed analysis [7, 13, 20]. Lester et al. has demonstrated that individual nAChR subunits can be labeled with fluorescent proteins for detection of individual subunit expression using live cell, fluorescence microscopy [21]. Using a combination of fluorescence confocal microscopy, total internal reflection fluorescence (TIRF) microscopy and advanced fluorescence techniques, such as Försters resonance energy transfer (FRET), it is possible to detect changes in membrane expression, trafficking, and receptor complex formation of fluorescent nAChRs [6, 22-23]. We hypothesized that selective labeling of an  $\alpha 5$  subunit would be possible for detection and observation of  $\alpha 5^*$  receptor populations.

The mouse *Chrna5* gene with partial 5' and 3' untranslated regions (UTR), as well as the mouse *Chrna5* genes with D/N mutation and partial 5' and 3' UTRs were generously provided by Dr. Jerry Stitzel at the University of Colorado Boulder. These genes were subcloned into pcDNA3.1(+) mammalian expression vectors. *Chrna5* is heavily enriched

for guanine and cytosine nucleotides in the 5' region, making polymerase chain reaction (PCR) extension of the entire gene difficult. Many efforts were made to optimize the PCR protocol for efficient and consistent extension of the entire gene. Those optimized methods are reported in appendix i. Several pcDNA3.1(+) constructs containing variations of the *Chrna5* gene with and without UTRs were constructed and are listed in table 1.

The nAChR M3-M4 loop is a preferred location for insertion of fluorescent protein (FP) tags [21-22]. It has been inferred from studies of other nAChR subunits that M3-M4 loop localized FP labels do not interfere with formation of the receptor complex, intracellular trafficking, or function of nAChRs [21]. Sequence alignment of mouse nAChR M3-M4 loops revealed that  $\alpha 5$  contains the shortest loop (50 amino acids), and concerns were raised that the insertion of a ~ 200 amino acid fluorescent protein such as GFP would produce steric interference, preventing efficient incorporation of the labeled subunit into a receptor complex or the proper trafficking of an  $\alpha 5^*$ -FP receptor to the plasma membrane. Consequently, several variants of  $\alpha 5$ -FP fusion products were constructed (see table 1).

Building on previous work by Lester et al., monomeric enhanced green fluorescent protein (mEGFP) was selected as the FP for insertion into the  $\alpha 5$  gene. mEGFP exhibits enhanced fluorescence over wild-type GFP (wtGFP) and also contains an alanine-to-lysine mutation at position 206 that prevents multimerization of GFP molecules [24-25]. These modifications make mEGFP more compatible with biological imaging experiments and FRET analysis. Two intrasubunit locations for mEGFP were selected within the  $\alpha 5$  M3-M4 loop.

**Table 1**

5' UTR	Sequence	Linker (A-G-A)	FP Insertion Site	Linker (G-A-G)	3' UTR	3'MUT	C – term FP
yes	Mouse $\alpha$ 5				yes		
	Mouse $\alpha$ 5						
	Mouse $\alpha$ 5 D398N						
yes	Mouse $\alpha$ 5		mEGFP 385		yes		
yes	Mouse $\alpha$ 5	yes	mEGFP 385	yes	yes		
yes	Mouse $\alpha$ 5		mGFP 378		yes		
	Mouse $\alpha$ 5	yes	mEGFP 378	yes			
	Mouse $\alpha$ 5	yes	mCherry 385	yes			
	Mouse $\alpha$ 5	yes	mCherry 378	yes	yes		
	Mouse $\alpha$ 5 D398N	yes	mEGFP 378	yes			
	Mouse $\alpha$ 5	yes	mEGFP 378	yes		yes	
	Mouse $\alpha$ 5 D398N	yes	mEGFP 378	yes		yes	
	Mouse $\alpha$ 5						mEGFP
	Mouse $\alpha$ 5 D398N						mEGFP

These locations were chosen due to their distance from the position of the identified SNP (amino acid 397 in the mouse protein, 398 in the human) and from identified trafficking motifs (see figure 1.1) [23, 26]. A flexible linker of alanine and glycine (A-G-A or G-A-G) was included with the inserted mEGFP sequence. Other  $\alpha$ 5-mEGFP fusion constructs with the mEGFP sequence fused to the c-terminal region of the  $\alpha$ 5 sequence

were also constructed using overlap PCR. Table 2 comprehensively displays all of the  $\alpha 5$ -mEGFP variants that have been used experimentally throughout the duration of this project.

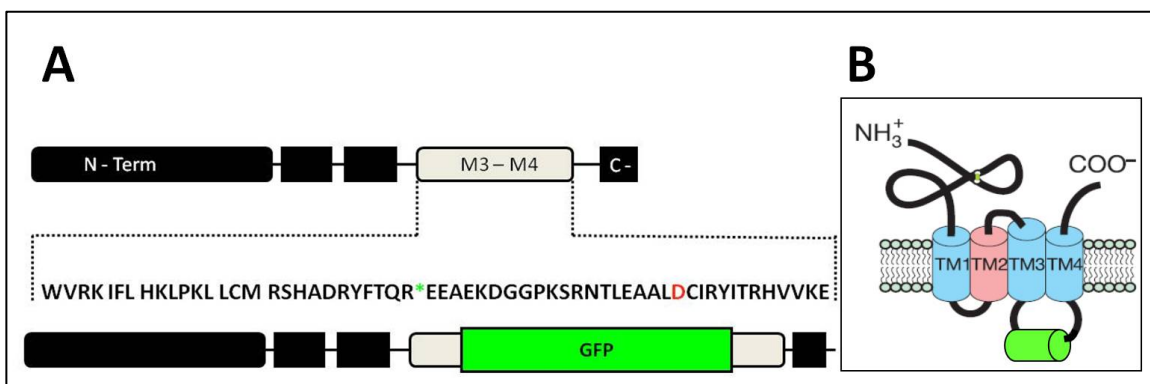


**Figure 1.1**

Schematic of the nAChR  $\alpha 5$  subunit.

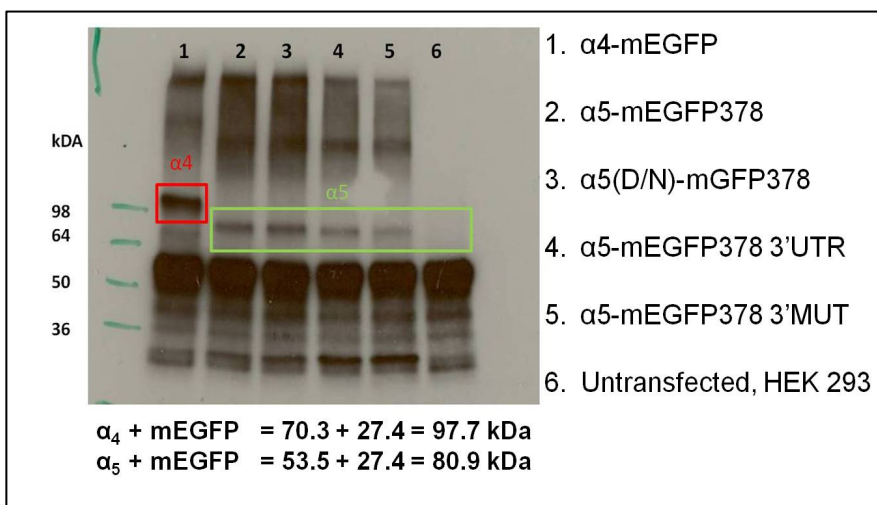
1.1A shows the amino acid sequence of the  $\alpha 5$  M3-M4 loop. Asterisk indicates position 358, one of the two intracellular loop locations for mEGFP insertion.

1.1B Shows an alternative view of the  $\alpha 5$  subunit, showing helical transmembrane domains and mEGFP barrel in the M3-M4 loop region (not to scale).

**Table 2**

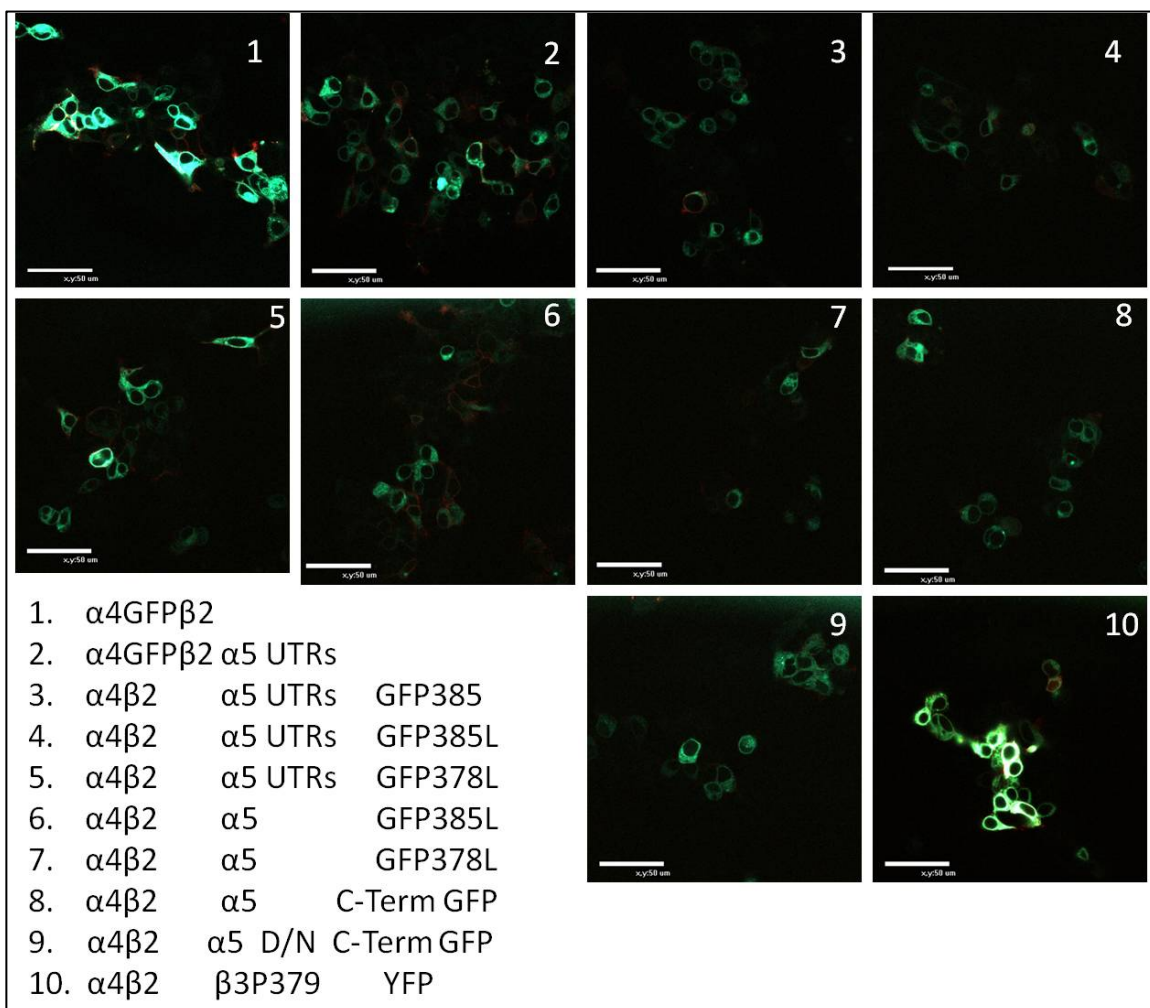
5'UTR	Mouse $\alpha 5$ Template	mEGFP Location	3'UTR
✓	wt	385	✓
	wt	378	✓
	wt	378	
	V280S	378	
	D398N	378	✓
	D398N	378	
	V280S D398N	378	

Full length expression of the  $\alpha 5$ -mEGFP fusion constructs was verified using Western blot.  $\alpha 5$ -mEGFP constructs were expressed in either HEK293 or HEK293-T cells and immunoprecipitated using a mouse anti-GFP antibody. Extracts were then separated by gel electrophoresis and blotted with a rabbit anti-GFP primary and goat anti-GFP-HRP secondary antibodies for visualization. Resultant bands were then compared to an expressed  $\alpha 4$ -mEGFP control (see figure 1.2).

**Figure 1.2**

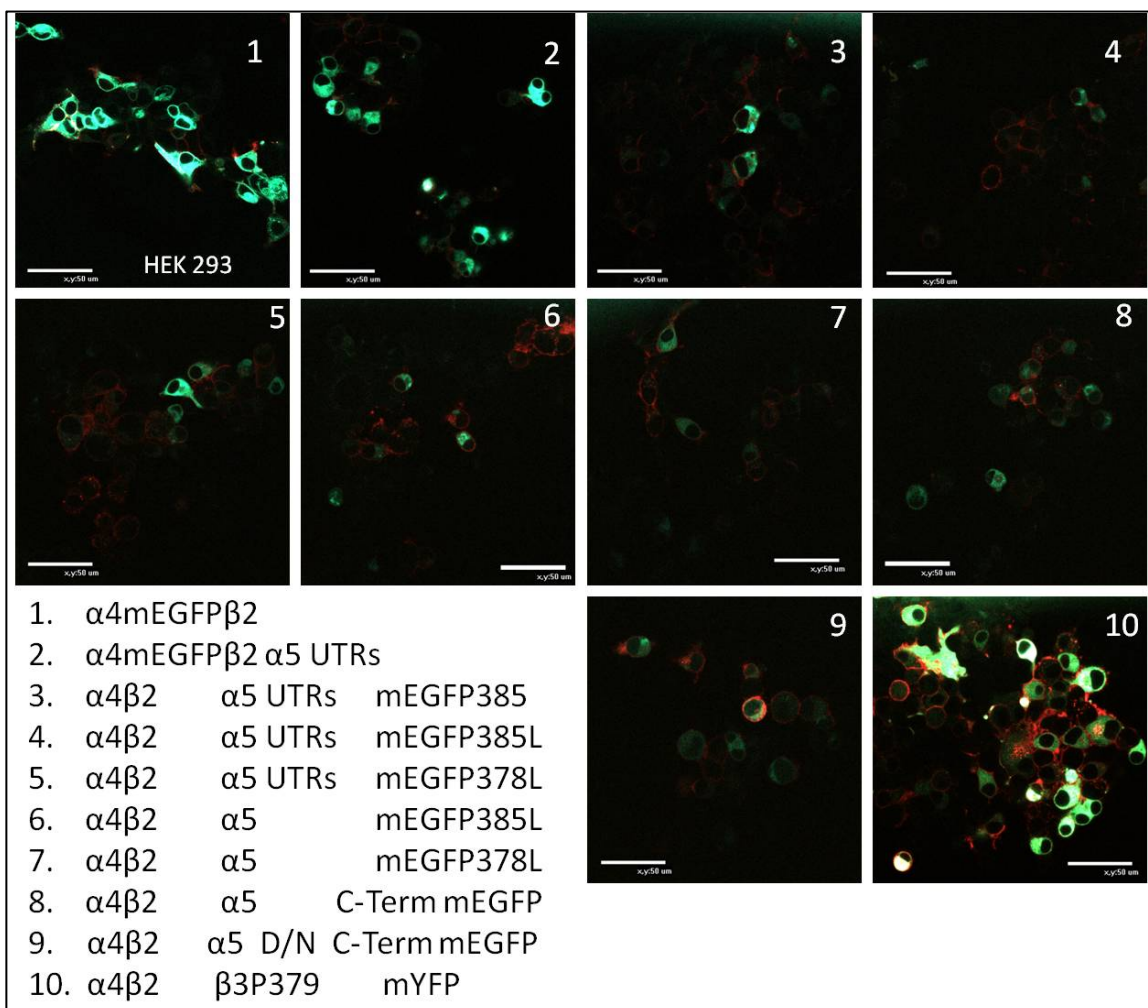
Western blot demonstrates full length (80.9 kDa) expression of  $\alpha_5$ -mEGFP constructs in HEK293 cells. Lane 1 contains  $\alpha_4$ -mEGFP as a positive control. Lanes 2-5 contain variants of  $\alpha_5$ -mEGFP. Lane 6 contains lysate from untransfected cells.

Next,  $\alpha_5$ -mEGFP constructs were assayed for fluorescence (see figure 1.3). Many of the fusion proteins were expressed in both N2a and HEK293 cell lines. N2a or HEK293 cells were transiently transfected with  $\alpha_5$ -mEGFP,  $\alpha_4$ , and  $\beta_2$  subunits and assayed for fluorescence using confocal microscopy. Fluorescence levels for all of the  $\alpha_5$ -mEGFP constructs were consistently low when compared to  $\alpha_4$ -mEGFP and  $\beta_3$ -mYFP controls. This lack of expression was a consistent challenge moving forward with investigations using these constructs. However,  $\alpha_5$ -mEGFP387, a DNA construct lacking the 5' and 3' UTR regions, with A-G-A and G-A-G flanking linker sequences, and with the mEGFP inserted at position 378 was ultimately chosen as the optimum construct for use in future experiments.



**Figure 1.3A**

Images of N2a cells expressing fluorescent nAChR constructs and a red fluorescent plasma membrane marker PM-mCherry. Images were taken 24 h post-transfection with a scanning confocal microscope after sample excitation with 488 nm laser. Images 1, 2, and 10 display images of HEK293 cell expressing  $\alpha 4$ -mEGFP or  $\beta 3$ -mYFP as positive controls for relative expression. Images 3 – 9 show the low relative fluorescence of the  $\alpha 5$ -mEGFP constructs.

**Figure 1.3B**

Images of HEK293 cells expressing fluorescent nAChR constructs and a red fluorescent plasma membrane marker PM-mCherry. Images were taken 24 h post-transfection with a scanning confocal microscope after sample excitation with 488 nm laser. Images 1, 2, and 10 display images cells expressing  $\alpha 4$ -mEGFP or  $\beta 3$ -mYFP as positive controls for relative expression. Images 3 – 9 show the low relative fluorescence of the  $\alpha 5$ -mEGFP constructs.

Intracellular assembly of  $\alpha 5$ -mEGFP378 ( $\alpha 5$ -mEGFP) with  $\alpha 4$  and  $\beta 2$  subunits to form an  $\alpha 4\beta 2\alpha 5$ -mEGFP receptor was evaluated using normalized Försters resonance energy transfer (NFRET). NFRET uses the distance dependence of energy transfer between a donor and acceptor fluorophore to measure interactions between proteins. Attention is paid to the theory of FRET and NFRET in chapter 4. FP labeled  $\alpha 4$  and/or  $\beta 2$  subunits were co-expressed in N2a cells, and NFRET measurements were performed. In this case the  $\alpha 5$ -mEGFP acted as the FRET donor, and a red fluorescent protein, mCherry, labeling the  $\alpha 4$  subunit, functioned as the FRET acceptor (see chapter 4) [6, 23, 26]. Low incidence of expression of the  $\alpha 5$ -mEGFP (15%) made finding cells expressing both  $\alpha 5$ -mEGFP and  $\alpha 4$ -mCherry at levels sufficient for FRET signal detection challenging, but we are able to demonstrate intracellular association of  $\alpha 5$ -mEGFP and  $\alpha 4$ -mCherry when co-expressed with  $\beta 2$  in transiently transfected N2a cells (figure 1.4).

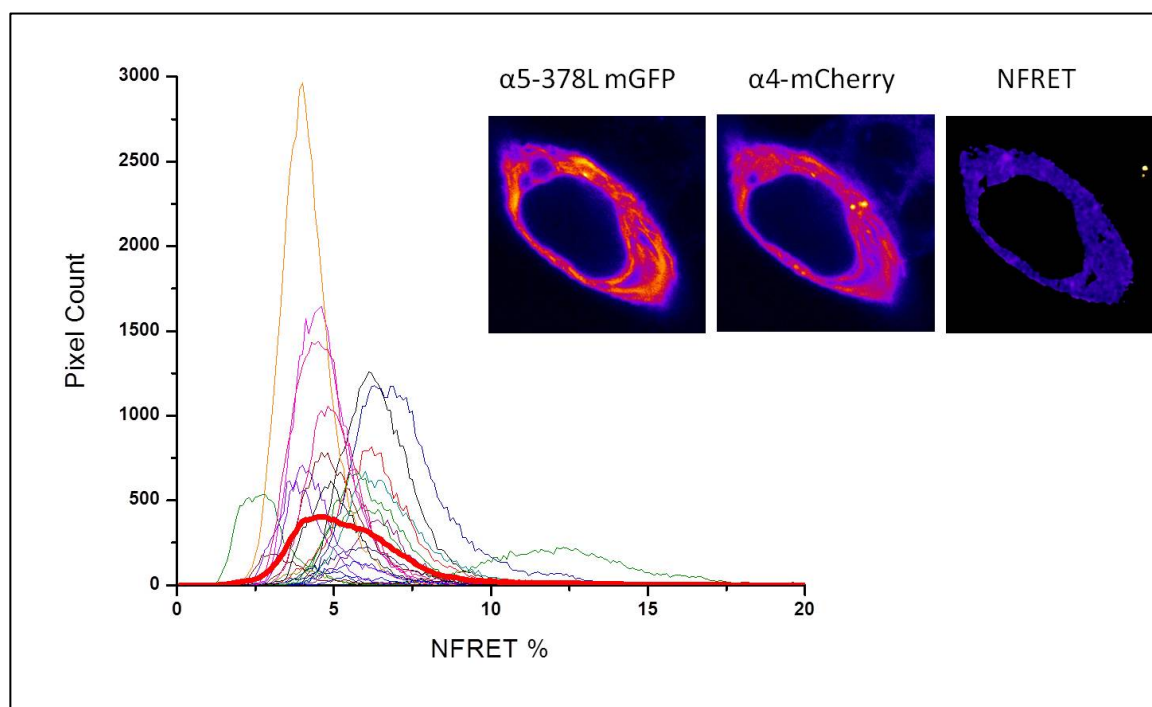


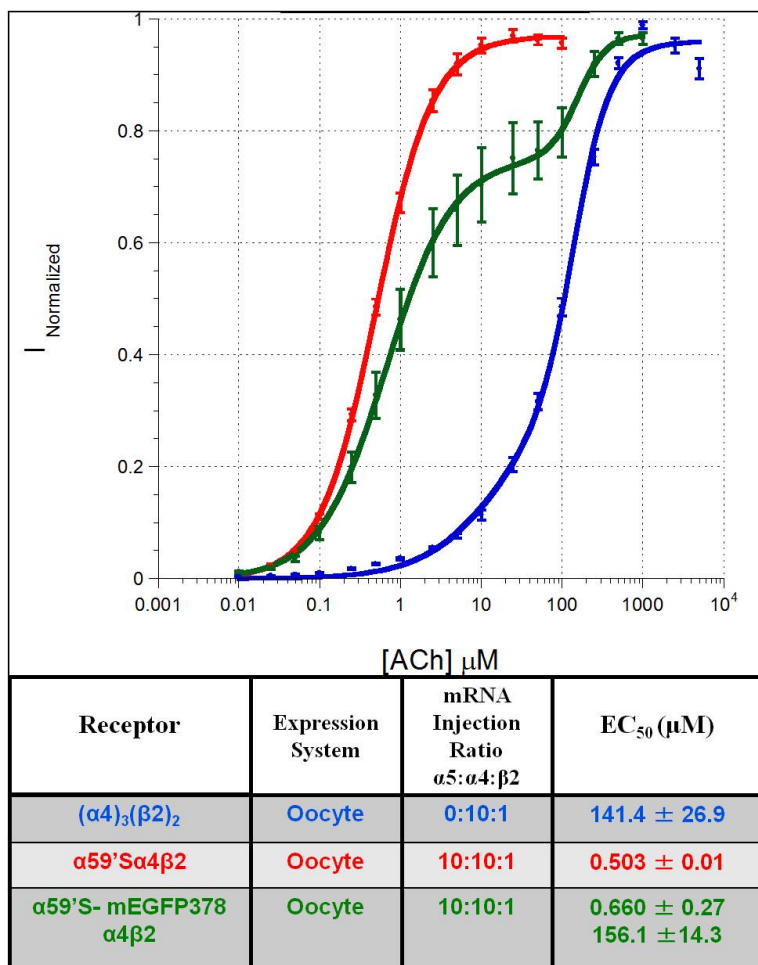
**Figure 1.4**

23 individual cell histograms of NFRET positive pixels in images of HEK293 cells expressing  $\alpha 5$ -mEGFP378,  $\alpha 4$ -mCherry, and  $\beta 2$  subunits. Bolded histogram describes the average of all 23 cells.

Boxes on the right display sample images of an HEK293 cell expressing  $\alpha 5$ -mEGFP378,  $\alpha 4$ -mCherry, and the associate NFRET values illustrated as a heat map of expression intensity.

Within the cell nAChRs, like other receptor complexes, are synthesized and assembled in the endoplasmic reticulum (ER). Once assembled, the complete pentameric complex is trafficked to the plasma membrane (PM) for insertion. It is understood that only complete nAChR pentamers reside in the PM. Functional response of  $\alpha 5$ -mEGFP $\alpha 4\beta 2$  receptors to agonist would confirm proper synthesis, incorporation, and trafficking of  $\alpha 5$ -mEGFP $\alpha 4\beta 2$  receptors. Electrophysiology on *Xenopus* oocytes expressing  $\alpha 5\alpha 4\beta 2$  receptors was performed in collaboration with Chris Marotta, and some results are reported in Marotta et al. [20]. Both  $\alpha 5\alpha 4\beta 2$  and  $(\alpha 4)_2(\beta 2)_3$  have a similar dose response to acetylcholine (ACh), and no pharmacological agents for selective activation of  $\alpha 5$  receptors have yet been reported.

Mutation of a conserved leucine (L) at the 9' position within a nAChR subunit confers "hypersensitivity" to agonist in receptors containing L9' mutant subunits [27-29]. Thus, 9' mutations can act as a reporter for subunit incorporation. Interestingly, the "accessory" subunits  $\alpha 5$  and  $\beta 3$  do not have the conserved amino acid at their 9' location. Both the  $\alpha 5$  and  $\beta 3$  subunit sequences have a valine (V) occupying the 9' position. Hypersensitive  $\beta 3$  subunits have been constructed by mutation of either the 9' or 13' positions [22]. To construct a potentially hypersensitive  $\alpha 5$  subunit, the 9'V at position 280 was mutated to an S to create  $\alpha 5V9'S$  and  $\alpha 5V9'S$ -mEGFP constructs. These constructs were then subcloned into the oocyte expression vector pGEMhe for use in electrophysiology experiments. Injection of  $\alpha 5V9'S$  mRNA with  $\alpha 4$  and  $\beta 2$  in a 10:10:1 ratio was sufficient to cause a leftward shift in dose response to ACh. We conclude that  $\alpha 5V9'S\alpha 4\beta 2$  receptors are formed, and the increase in receptor sensitivity indicates that the 9'S mutation can act as a reporter for  $\alpha 5$  incorporation (see figure 1.5). Injection of  $\alpha 5V9'S$ -mEGFP mRNA with  $\alpha 4$  and  $\beta 2$  in a 10:10:1 ratio results in a biphasic dose response to ACh. This shift indicates that the fluorescently labeled subunit is incorporated into an  $\alpha 5V9'S$ -mEGFP $\alpha 4\beta 2$  receptor, but subunit incorporation may not be as efficient.

**Figure 1.5**

Acetylcholine dose response curves from  $(\alpha 4)_3(\beta 2)_2$  –bottom curve  
 $\alpha 59's$ -mEGFP $\alpha 4\beta 2$ -middle curve  
 $\alpha 59'S\alpha 4\beta 2$  –top curve.  
 Receptors expressed in *Xenopus* oocytes and recorded with an OpusExpress.

Table below describes the mRNA injection ratio of each subunit and calculated  $EC_{50}$  value from the dose response curve.

With these data we are able to demonstrate construction of a functional fluorescent  $\alpha 5$ -mEGFP subunit. Complete protein expression was verified using IP and Western blot.  $\alpha 5$ -mEGFP was shown to be fluorescent via heterologous expression in transiently transfected N2a, HEK293, and HEK293-T cells using fluorescence confocal microscopy. Expression of fluorescent  $\alpha 5$  is consistently low compared to other fluorescent  $\alpha$  subunits, and low expression of many  $\alpha 5$ -mEGFP constructs has been observed in N2a and HEK293 clonal cell lines. Functional verification of  $\alpha 5$ -mEGFP was performed by oocyte electrophysiology, and the optimized  $\alpha 5$ -mEGFP construct,  $\alpha 5$ -mEGFP378, was selected for use in additional experiments.

## Chapter 2

### *Investigation into miR-346 Regulation of the nAChR $\alpha 5$ Subunit*

MicroRNA's (miRNAs) are small (< 25 base pairs), single stranded, non-coding RNAs that regulate gene expression at the post transcriptional level. Mature miRNAs form loose base pair interactions with the UTR regions of their target mRNA transcripts. This can lead to degradation and impaired translation. Because the base pair interaction between miRNA and mRNA target are imperfect, one miRNA may regulate many gene products [30]. Many miRNA's are expressed in spatially and temporally restricted patterns, and miRNA regulation has been associated with almost every cellular process, including cancer, immune response, and cellular degeneration [30]. miRNAs are also known to play a large part in development, acting as "switches" to control critical timing dependent processes such as organogenesis and neural development [30].

A few nAChRs are thought to be regulated by miRNAs, but no in-depth investigation has been undertaken. In *C. elegans*, a conserved miRNA, miR-1, regulates the expression of two nAChR muscle subtypes that are important for synaptic transmission at the neuromuscular junction [31]. Preliminary screening of a commercially available library of orphan miRNAs against luciferase-based reporter constructs with murine nAChR 3'UTRs have revealed several candidate miRNA-nAChR interactions (unpublished work by Eric Hogan, University of Massachusetts). A single miRNA, miR-346 was shown to inhibit luminescence when luciferase was coupled to the  $\alpha 5$  3'UTR or  $\alpha 10$  3'UTR (see figure 2.1).

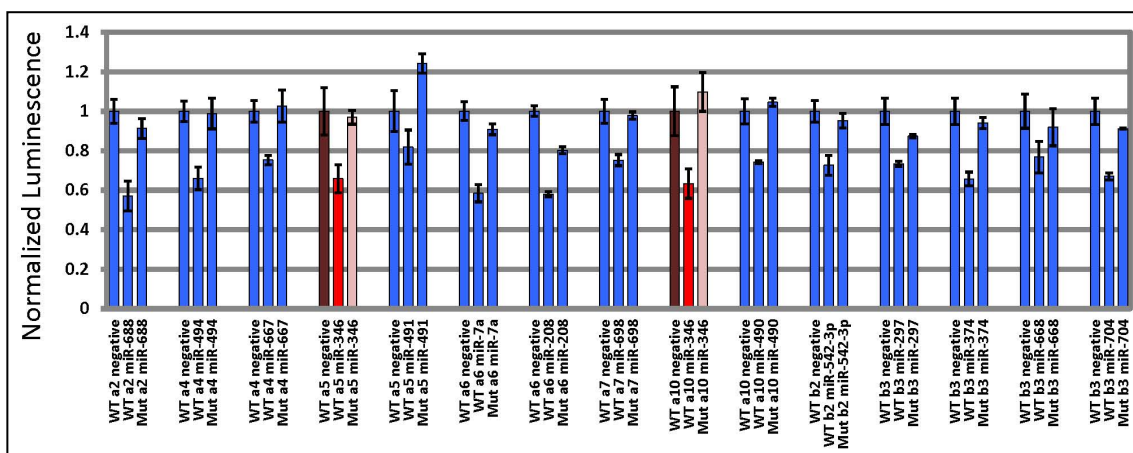


**Figure 2.1.** Results of luciferase screen of orphan miRNA library against nAChR 3'UTRs. Subunits affected by miR-346 are highlighted in red. Both  $\alpha 5$  and  $\alpha 10$  3'UTR constructs displayed a 30% reduction of luminescence in cells co-expressed with miR-346, but not when the 3'UTR contained mutated recognition sequences. (data from Hogan et al.)

Follow-up studies identified the miRNA recognition element recognized by miR-346 in the  $\alpha 5$  and  $\alpha 10$  3' UTR as ACAGGCAGACA. Mutations to this sequence in both the  $\alpha 5$  and  $\alpha 10$  3' UTR resulted in no effect on luciferase activity when miR-346 was present (figure 2.2). With the interaction between miR-346 and  $\alpha 5$  and  $\alpha 10$  3' UTRs firmly established, we next examined miR-346 regulation of the  $\alpha 5$  protein as expressed in clonal cells transiently transfected with  $\alpha 5$  subunits.

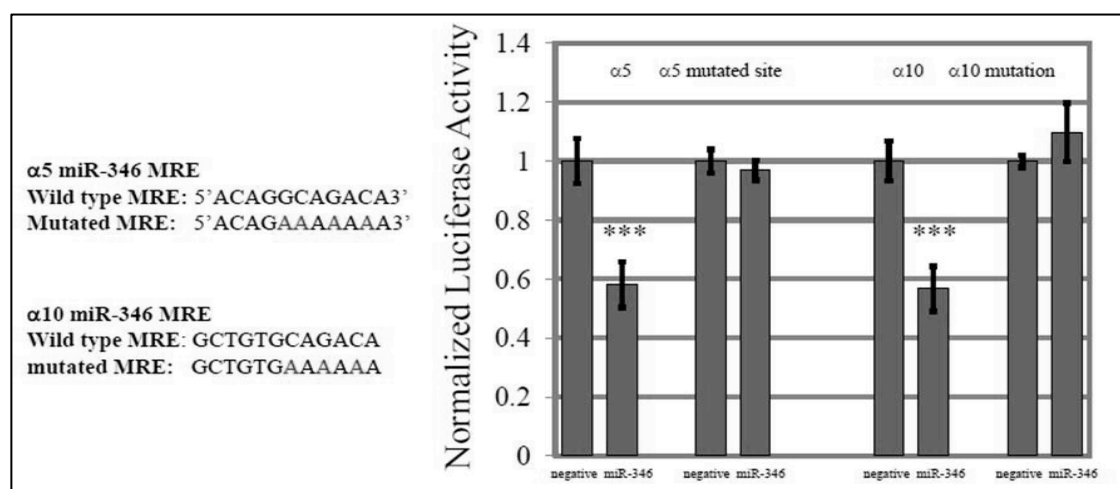


**Figure 2.2**

Site directed mutagenesis of predicted miR-346 binding sites in the 3' UTR of  $\alpha 5$  and  $\alpha 10$  was carried out in the context of MIR-REPORT-Luciferase. Mutated sequences are shown on the right. MRE = miRNA recognition element. Bars indicate mean  $\pm$  SEM. Student t-test \*\*\* $p \leq 0.001$  (data from Hogan et al.)

In collaboration with Hogan et al. in the Tapper Lab at the University of Massachusetts,  $\alpha 5$ -mEGFP was selected as the reporter construct for further investigations. The complete mouse  $\alpha 5$  wt 3'UTR (3'UTR) or 3'UTR with mutated miR-346 MRE (3'MUT) were subcloned into the  $\alpha 5$ -mEGFP378 and  $\alpha 5$ D/N-mEGFP378 plasmid constructs (see table 1). Expression analysis of the constructed  $\alpha 5$ -mEGFP fusion proteins was performed using HEK293-T cells transiently transfected with  $\alpha 5$ -mEGFP,  $\alpha 5$ -mEGFP-3'UTR,  $\alpha 5$ -mEGFP-3'MUT,  $\alpha 5$ D/N-mEGFP,  $\alpha 5$ D/N-mEGFP-3'UTR, or  $\alpha 5$ D/N-mEGFP-3'MUT (figure 2.3). Statistical differences in total fluorescence were detected between  $\alpha 5$ -mEGFP and  $\alpha 5$ D/N-mEGFP, and also between  $\alpha 5$ -mEGFP and  $\alpha 5$ D/N-mEGFP-3'MUT (t-test,  $p = 0.05$ ). Interestingly, there was no significant difference in fluorescence between  $\alpha 5$ -mEGFP and  $\alpha 5$ D/N-mEGFP-3'UTR.

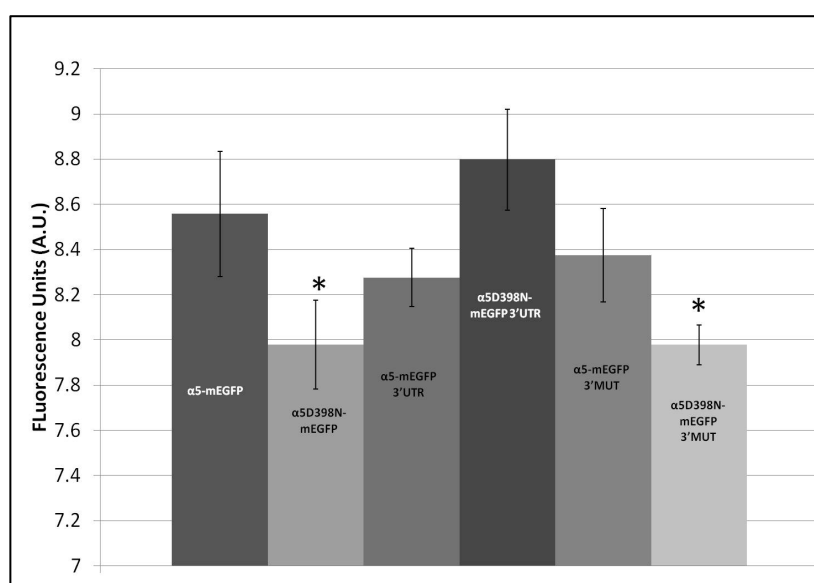


**Figure 2.3**

Relative fluorescence of  
 $\alpha 5$ -mEGFP  
 $\alpha 5$ D398N-mEGFP  
 $\alpha 5$ -mEGFP3'UTR  
 $\alpha 5$ D398N-mEGFP3'UTR  
 $\alpha 5$ -mEGFP3'MUT  
 $\alpha 5$ D398N-mEGFP 3'MUT  
 expressed in HEK293T cells  
 and assayed for fluorescence  
 using a standard fluorometer.

Asterisks indicate significant reduction in expression compared to  $\alpha 5$ -mEGFP, by t-test,  $p \leq 0.05$

Due to their small size and single stranded nature, miRNAs are highly unstable [30]. A precursor form of the desired miRNA is used for transfection to prevent degradation of the desired miRNA. Once inside the cell, the Pre-miR is processed by

endogenous proteins to create a mature miRNA strand. At high concentrations, non specific interactions of miRNA with mRNA transcripts can occur. These interactions may lead to regulatory effects on non-target sequences. We sought to optimize the concentration of miR-346 precursor (Pre-miR-346) necessary for regulation of  $\alpha 5$ -mEGFP-3'UTR.  $\alpha 5$ -mEGFP-3'UTR or  $\alpha 5$ -mEGFP-3'MUT were co-transfected with varying concentrations of Pre-miR346 for expression in HEK293-T cells. Results show that 1 nM Pre-miR-346 is the optimum concentration for use in further experiments (figure 2.4).

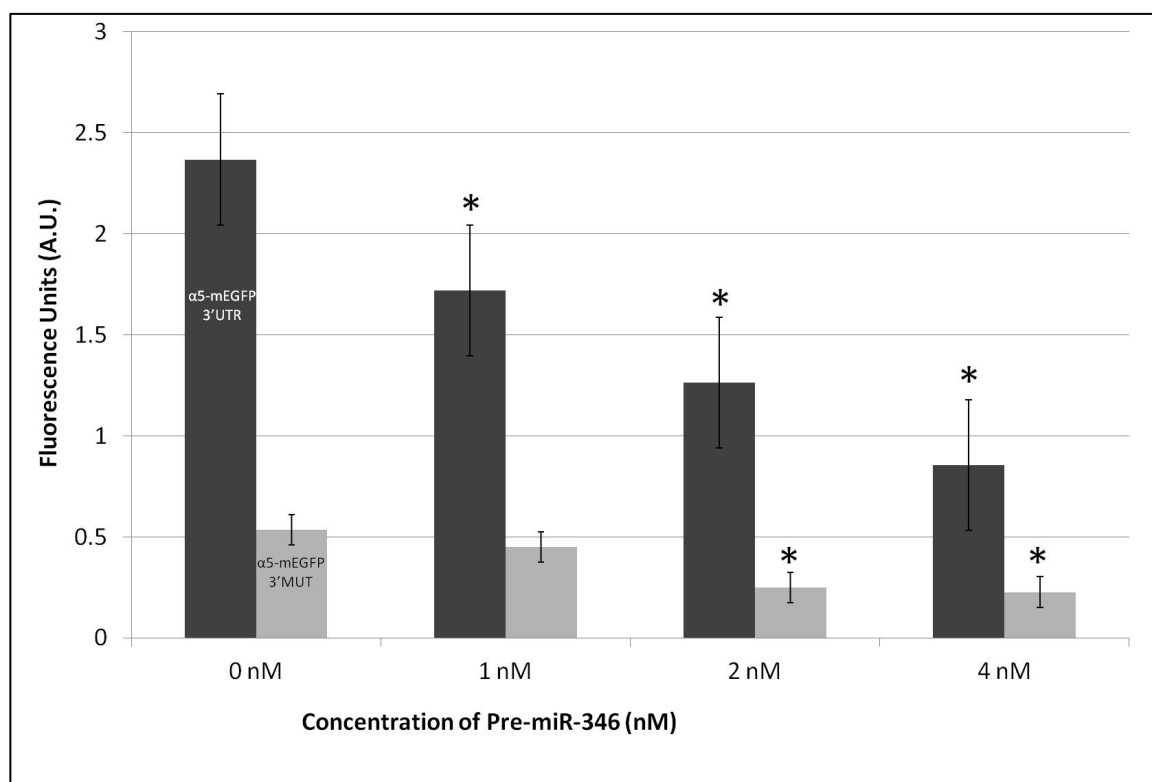


**Figure 2.4**

Bar graph illustrating resultant fluorescence from transfections of  $\alpha 5$ -mEGFP-3'UTR (dark grey) or  $\alpha 5$ -mEGFP-3'MUT (light grey) with varying concentrations of Pre-miR-346. Asterisk indicates significant variation ( $p \leq 0.05$ ) from 0nM values. 1 nM was selected as the optimal concentration of Pre-miR346 because at that concentration significant reduction in  $\alpha 5$ -mEGFP-3'UTR but not in  $\alpha 5$ -mEGFP-3'MUT was observed.

$\alpha 5$ -mEGFP-3'UTR was then co-transfected with 1 nM of Pre-miR346, a scrambled miRNA precursor, or  $\alpha 5$  siRNA. Cells were assayed for fluorescence intensity using a

fluorescent plate reader 24 h post-transfection. Preliminary results from Hogan et al. showed a 50% reduction in  $\alpha 5$ -mEGFP-3'UTR expression when co-transfected with Pre-miR-346 (figure 2.5).

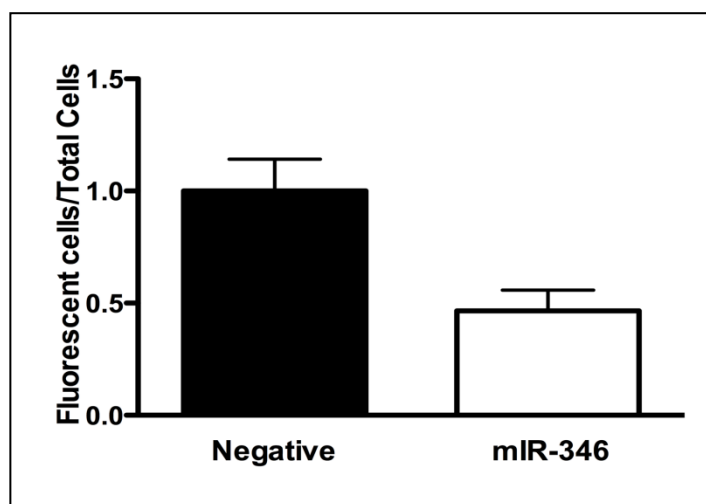


**Figure 2.5**

Results of fluorescence assay of HEK293-T cells transiently transfected with  $\alpha 5$ -mEGFP-3'UTR and either 1nM of scrambled negative control or 1nM Pre-miR-346.

Fluorescence is reduced by almost 50% when Pre-miR-346 is transfected with  $\alpha 5$ -mEGFP-3'UTR (data from Hogan et al.)

However, additional experiments using  $\alpha 5$ -mEGFP and  $\alpha 5$ -mEGFP-3'MUT as positive and negative control, respectively, were unable to repeat these results. Figure 2.6 shows the consistent lack of response of the various  $\alpha 5$ -mEGFP constructs to different transfection conditions. Reduction in fluorescence of  $\alpha 5$ -mEGFP3'UTR upon addition of miR-346 was not significant and additionally, greater reduction of  $\alpha 5$ -mEGFP3'UTR expression was seen when  $\alpha 5$ -mEGFP3'UTR was co-transfected with a scrambled Pre-miR sequence than in the Pre-miR-346 condition. Obviously, more experiments are needed to determine specific regulation of  $\alpha 5$ -mEGFP3'UTR via direct, sequence-specific interaction between miR-346 and the  $\alpha 5$  3'UTR.

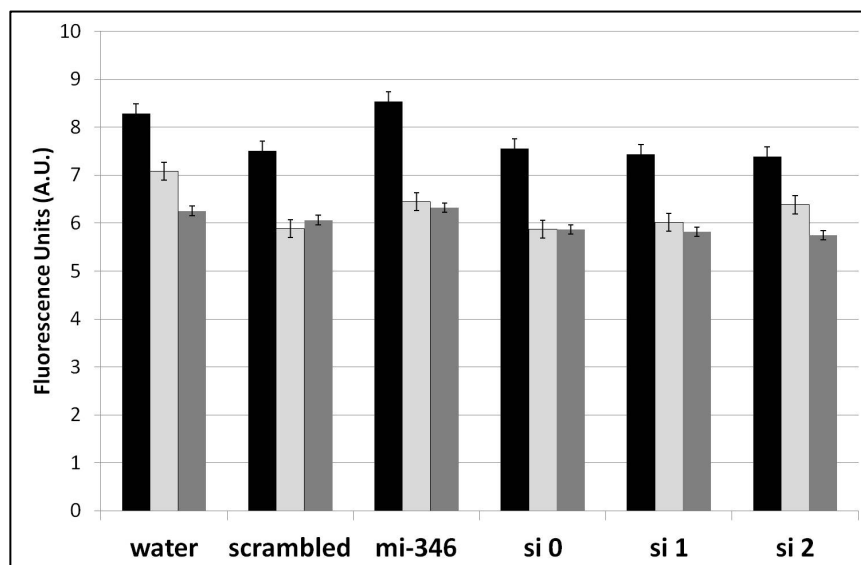


**Figure 2.5**

Bar graph representing relative fluorescence of  $\alpha 5$ -mEGFP (black)  $\alpha 5$ -mEGFP 3'UTR (light grey)  $\alpha 5$ -mEGFP 3'MUT (dark grey) after co-transfection with (right to left) water, scrambled Pre-miR, Pre-miR-346, or commercially available siRNAs to  $\alpha 5$  siRNA0, siRNA2, siRNA.

$\alpha 5^*$  receptors have been implicated in developmental changes in activation and morphology of the medial prefrontal cortex (mPFC). The mPFC is responsible for decision making and attention as well as other higher-order cognitive processes. Cholinergic inputs to the cortex appear early in brain development and are widespread in rats by the third week of post-natal life [32]. There is a corresponding developmental peak in nicotinic current response to ACh in rodent mPFC layer VI neurons that is mediated by  $\alpha 5^*$  receptors and occurs during a crucial period of cortical circuit refinement [10, 32-33]. Nicotinic stimulation during this period can modulate the retraction and maturation of neuronal processes [32].  $\alpha 5^*$  receptors are known to be enriched in layer VI of the mPFC and it has recently been discovered that proper expression of the  $\alpha 5$  subunit in this area during development plays an important role in normal attention behavior in adult mice [10]. Work by Leslie et al. examining expression of  $\alpha 5$  mRNA in rats indicates that there may be a global reduction in  $\alpha 5$  mRNA after post-natal day 10 [34]. We hypothesize that this down regulation of  $\alpha 5$  mRNA may be due to regulation by miRNAs such as miR-346.

In this chapter we have identified a miRNA, miR-346, that may be involved in regulation of nAChR expression. This miRNA is upregulated in adult mouse brain after chronic nicotine exposure, and a reduction in luminescence of a luciferase reporter construct fused to the  $\alpha 5$  3'UTR in the presence of miR-346 is reported. More investigation is necessary to determine the nature of the biological interaction between miR-346 and  $\alpha 5$ . However, preliminary experiments suggest that fluorescence of  $\alpha 5$ -mEGFP-3'UTR is reduced in the presence of 1 nM Pre-miR-346. Data presented here lays the foundation for investigation of miRNA regulation of nAChRs and specific regulation of  $\alpha 5$  by miR-346. Elucidating the role of miR-346 in regulation of  $\alpha 5$  expression could have implications for brain development and disease states.

### Chapter 3

#### *Expression of $\alpha 5$ -mEGFP in Mouse Cortical Neurons*

Subcellular localization of the neuronal nAChR subtypes  $\alpha 4\beta 2$  and  $\alpha 4\beta 4$  depends on the  $\beta$  subunit. Signal sequences in the M3-M4 loop of  $\beta$  nAChRs bind protein factors to enable or inhibit forward trafficking for expression on the cell membrane. The M3-M4 loops of some subunits, like  $\beta 4$ , contain forward trafficking signals that contribute to the abundant expression of receptors containing those subunits at the cell surface [35]. However, many subtypes, such as those that contain the  $\beta 2$  subunit, are primarily retained in the ER. For these receptors, molecular chaperones such as nicotine may aid in surface expression [23, 36]. The presence of these intracellular trafficking sequences may act as an intra-receptor level of nAChR regulation. The  $\alpha 4\beta 2$  receptor can exist in two stoichiometries, one of which traffics more readily to the membrane [23]. This difference in trafficking between stoichiometries may be partially due to the number of beta subunits contained in the receptor. An RRQR retention motif has been identified in the M3-M4 loop of the nAChR  $\beta 2$  subunit. The  $(\alpha 4)_3(\beta 2)_2$  receptor traffics to the membrane more easily than  $(\alpha 4)_2(\beta 2)_3$  because the  $(\alpha 4)_2(\beta 2)_3$  stoichiometry contains more beta subunits and therefore more RRQR signals [23, 37]. nAChRs may also use incorporation of accessory subunits such as  $\alpha 5$  and  $\beta 3$  to modulate trafficking and expression.

Examination of the  $\alpha 5$  M3-M4 loop identified a forward trafficking IFL amino acid motif beginning at position 354 and a LCM motif at position 364. I/LXM motifs, where X can be any amino acid, have been associated with vesicular export from the endoplasmic reticulum. The I/LXM sequence interacts with a surface groove of Sec24D, a major component of COPII vesicles, for efficient cargo packaging [38]. Presence of Sec24D

targeting sequences in the  $\alpha 5$  subunit imply that incorporation of an  $\alpha 5$  into a parent receptor may encourage trafficking of the  $\alpha 5^*$  receptor to the plasma membrane via interaction with Sec24D and other COPII machinery. When  $\alpha 5$  is incorporated into an  $\alpha 4\beta 2$  receptor, the receptor stoichiometry becomes fixed as  $\alpha 5(\alpha 4\beta 2)_2$ . This  $\alpha 5(\alpha 4\beta 2)_2$  receptor contains two ER retention RRQR signals from the  $\beta 2$  subunits and one IFL motif in the M3-M4 loop of the  $\alpha 5$  subunit. We hypothesized that due to the reduction in retention sequences and the addition of a forward trafficking signal  $\alpha 5\alpha 4\beta 2$  receptors may be more easily expressed on the cell membrane than  $\alpha 4\beta 2$  receptors.

To assay whether  $\alpha 5\alpha 4\beta 2$  receptors are trafficked differently than  $\alpha 4\beta 2$  receptors, we first expressed these receptors heterologously in clonal cell lines N2a and HEK293. Cells were imaged live, 48 h post-transfection, at 37 °C with a Nikon C1 scanning confocal microscope. In all fluorescence experiments the percentage of cells with detectable  $\alpha 5$ -mEGFP fluorescence is low when compared to  $\alpha 4$ -mEGFP and  $\beta 3$ -mYFP controls. Even after optimization of transfection, expression, and imaging protocols,  $\alpha 5$ -mEGFP fluorescence remained  $\leq 50\%$  of control subunit levels. It is possible that like  $\alpha 7^*$  receptors, whose expression is significantly enhanced by co-expression with the chaperone protein Ric-3,  $\alpha 5^*$  receptors rely on endogenous protein chaperones or other factors for optimal expression, and  $\alpha 5$ -mEGFP may be more efficiently expressed in primary cells [39]. To test this hypothesis,  $\alpha 5$ -mEGFP was expressed in primary cultures of mouse neurons.

$\alpha 5$ -mEGFP plasmid DNA was transiently transfected into mouse cortical neurons alongside unlabeled  $\alpha 4$  and  $\beta 2$  subunits. Due to the difficulty of imaging primary neurons, cells expressing nAChRs were fixed with 4% paraformaldehyde (PFA) before

imaging. 48 h post-transfection cells were fixed, washed with 1% phosphate buffered saline (PBS), and imaged in PBS at room temperature after excitation with a 488nm laser. Images were spectrally unmixed against control spectra for mEGFP and background controls. When transfected with only  $\alpha 4$ -mEGFP and  $\beta 2$  plasmid DNA, mouse e17 cortical neurons express  $\alpha 4$ -mEGFP $\beta 2$  with a transfection efficiency of approximately 10% (figure 3.1). When  $\alpha 5$ -mEGFP is transfected with unlabeled  $\alpha 4$  and  $\beta 2$  subunits, very low intensity of  $\alpha 5$ -mEGFP fluorescence is seen. In addition to reduced fluorescence, a cell death rate of over 50% is observed. Unlike  $\alpha 4$ -mEGFP,  $\alpha 5$ -mEGFP exhibits low intensity fluorescence that is confined to the cell bodies (see figure 3.1B). Interestingly, when a red fluorescent  $\alpha 4$ -mCherry is transfected with green fluorescent  $\alpha 5$ -mEGFP and unlabeled  $\beta 2$ , all detected fluorescence, not just that from  $\alpha 5$ -mEGFP, is confined to the cell body (figure 3.1D). This is not true when fluorescent  $\alpha 4$  subunits are transfected with unlabeled  $\beta 2$  subunits alone (figure 3.1C).

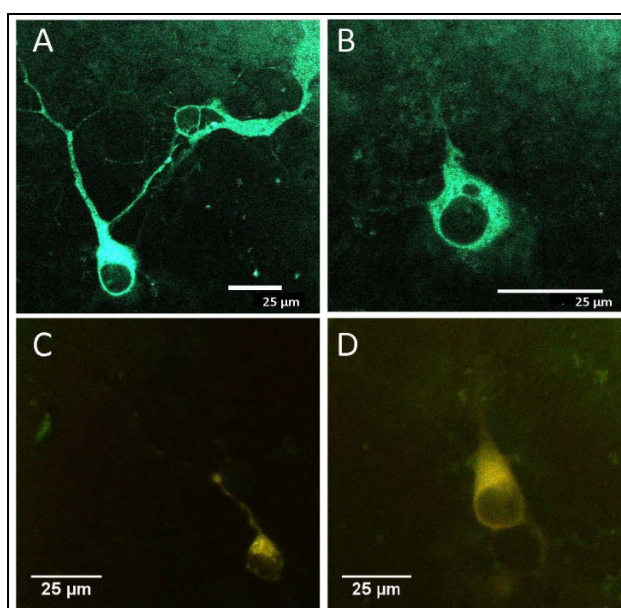


**Figure 3.1**

Mouse e17 cortical neurons expressing fluorescent nAChRs. Cells were transfected after 6 days in culture, fixed with 4% PFA and imaged 48 h post transfection. Samples were exposed to 488 nm (mEGFP) or 561 nm (mCherry) laser excitation and spectrally unmixed against control spectra for mEGFP and mCherry.

Scale = 25 microns

A)  $\alpha 4$ -mEGFP $\beta 2$  – fluorescence is fairly bright and extends into the processes. Laser intensity = 15%.

B)  $\alpha 5$ -mEGFP $\alpha 4\beta 2$  – fluorescence is dim and restricted to the cell body. Laser intensity = 35%

C)  $\alpha 4$ -mEGFP $\alpha 4$ -mCherry $\beta 2$  – overlay of images obtained using 488nm and 561 nm excitation. Laser intensity = 15%.

D)  $\alpha 5$ -mEGFP $\alpha 4$ -mCherry $\beta 2$  – overlay of images obtained using 488 nm and 561 nm excitation. Laser intensity = 35% and 15%, respectively.

We see that fluorescence from  $\alpha 4$ -mEGFP is distributed into the neuronal processes, but when the  $\alpha 5$  subunit is present, fluorescence is restricted to the cell body. It is possible that insertion of a fluorophore disrupted the efficiency of expression of  $\alpha 5$ -mEGFP. However, It is interesting to note that it is not the presence of the mEGFP in the intracellular loop that contributes to the expression problem.  $\alpha 5$ -mEGFP subunits constructed such that the mEGFP has been fused to the extracellular C-terminal domain of the  $\alpha 5$  subunit, leaving the M3-M4 loop clear of any manipulation were also transiently transfected into mouse cortical neurons with the same lack of success.

Given the high rate of cell death, attempts were made to optimize the neuronal transfection protocol. It was found that transfecting neurons in a lower volume of growth media (0.5 mL), combined with complete replacement of cellular medium following 4 h 37 °C incubation with the lipofection-DNA complex, greatly enhanced both transfection efficiency and cell viability (see appendix ii for complete optimized protocol). This optimization has eliminated the need for fixed cell imaging techniques. Using the CO<sub>2</sub> buffering Leibovitz media in the absence of phenol red, a small 37 °C incubator installed on the microscope stage, and a heating unit that warms the objective itself to 37 °C, it is possible to maintain live cell health during an imaging session for upwards of 1 h before apoptotic phenotypes are observed.

Figure 3.2A shows the poor expression and low fluorescence previously seen in the fixed neurons transiently transfected with  $\alpha 5$ -mGFP  $\alpha 4$   $\beta 2$  receptor subunits. The multiple cells in the single imaging field shown in figure 1C illustrate the improvements to the transfection efficiency over those previously used, and increased expression and visualization of the  $\alpha 5$ -mEGFP subunit after optimization of culture, transfection, and

imaging conditions. It is also important to note the increased fluorescence intensity and the improved distribution of fluorescence of the cells in shown in figure 3.2B and 3.2D when compared to the fixed cell shown in 3.2A. Improved transfection and cell culturing methods have allowed us to visualize more than just the cell soma. Figures 3.2B and 3.2D show that  $\alpha 5$ -mEGFP expression in live neuronal culture extends from the soma into both primary and secondary processes of the neuron.

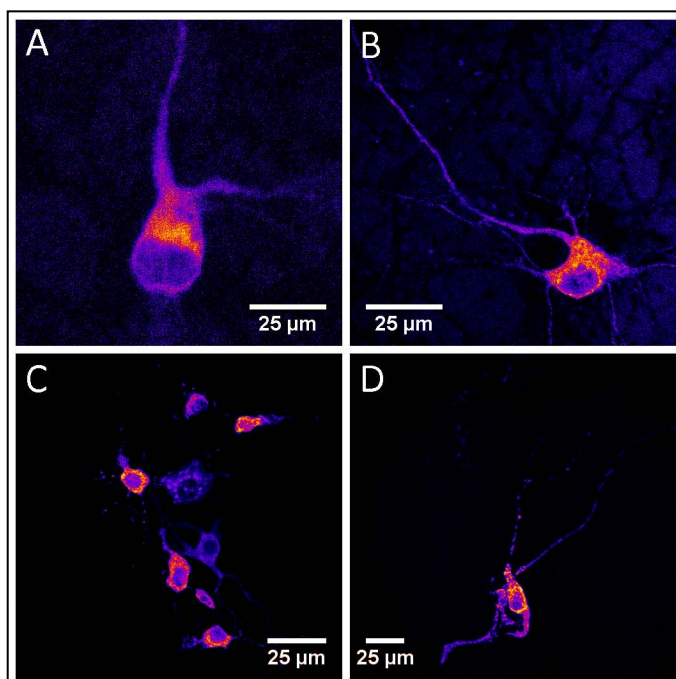


**Figure 3.2**

Mouse e17 cortical neurons expressing  $\alpha 5$ -mEGFP. Cells were transfected after 6 d in culture and imaged 24 h post-transfection. All images were taken with a scanning confocal microscope after excitation with 488 nm laser.

A. Expression of  $\alpha 5$ -mEGFP $\alpha 4\beta 2$  using non-optimized transfection protocol. Image was taken after fixation with 4% PFA, 24 h post-transfection.

B and D. Expression of  $\alpha 5$ -mEGFP $\alpha 4\beta 2$  under optimized cell culture and transfection protocol. Cells were imaged live, without fixation, 48 h post-transfection.

C. Widefield image of multiple fluorescent neurons in a dish illustrates the significant improvements in transfection achieved using the optimized protocol.

We know from previous experiments performed in HEK293 and N2a cells that  $\alpha 5$ -mEGFP or  $\alpha 5D398N$ -mEGFP subunits co-localize with  $\alpha 4$  and  $\beta 2$  receptor subunits (chapter 4).  $\alpha 5$ -mEGFP or  $\alpha 5D398N$ -mEGFP subunits also form functional receptors with  $\alpha 4$  and  $\beta 2$  receptor subunits in frog oocytes (chapter 1). The improvements made to experimental techniques have allowed us to ask whether  $\alpha 5$ -mEGFP or  $\alpha 5D398N$ -mEGFP subunits co-localize with  $\alpha 4$  and  $\beta 2$  receptor subunits in primary cell cultures. Figure 3.3 shows example images of co-transfection experiments with  $\alpha 5$ -mEGFP or  $\alpha 5D398N$ -mEGFP,  $\alpha 4$ -

mCherry, and unlabeled  $\beta 2$  subunits. This is the first reported expression of a mutant  $\alpha 5 D 3 9 8 N$ -mEGFP subunit in mouse neurons.

As stated in the introduction, the SNP rs16969968 encodes a D to N substitution in the M3-M4 loop of the  $\alpha 5$  subunit at position 398 and is associated with increased risk for nicotine dependence in humans [18]. It was hypothesized that the M3-M4 loop localization of the D398N mutation may contribute to changes in intracellular trafficking or localization of the mutant protein. Co-transfection experiments did not reveal any differences in localization between  $\alpha 4$ -mCherry and expressed  $\alpha 5$ -mEGFP and  $\alpha 5 D 3 9 8 N$ -mEGFP subunits (figure 3.3). This could indicate proper expression and assembly of  $\alpha 5$ -mGFP,  $\alpha 4$ -mCherry, and  $\beta 2$  into  $\alpha 5$ -mGFP $\alpha 4$ -mCherry $\beta 2$  receptors; unfortunately, no obvious differences in expression were seen upon introduction of the  $\alpha 5 D 3 9 8 N$ -mEGFP subunit.

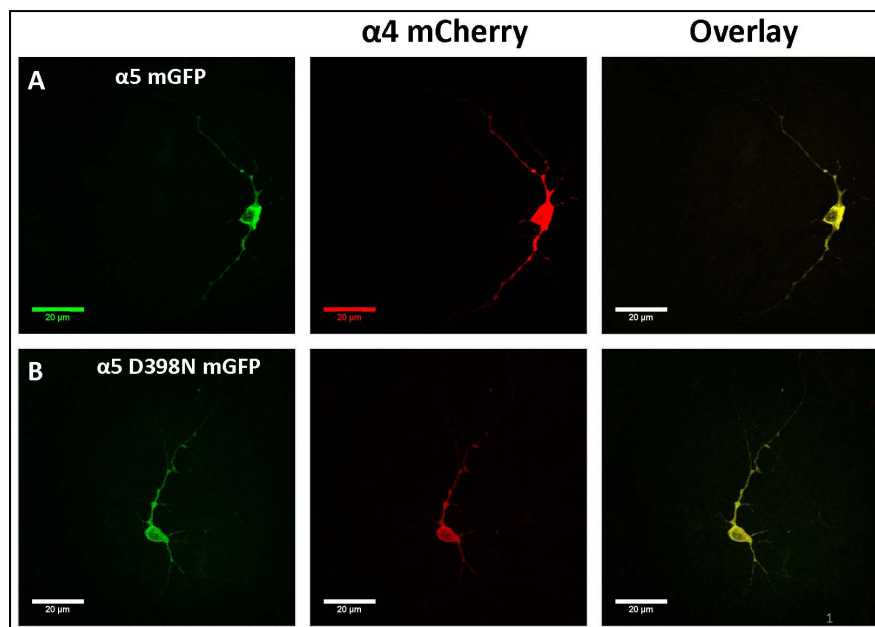
**Figure 3.3**

**A.** False color images (left to right) of  $\alpha 5$ -mEGFP  $\alpha 4$ -mCherry, and an overlay of the  $\alpha 5$ -mEGFP  $\alpha 4$ -mCherry images.

**B.** False color images (left to right) of  $\alpha 5 D 3 9 8 N$ -mEGFP  $\alpha 4$ -mCherry, and an overlay of the  $\alpha 5$ -mEGFP  $\alpha 4$ -mCherry images.

All images are max-intensity projections of 1 micron step size z-stacks. Imaging was performed with a scanning confocal microscope after sample excitation by 488 nm for the mEGFP (green) or 561 nm for mCherry (red).

All scale bars 20 microns.



Co-localization studies performed on cells expressing  $\alpha 5$ -mEGFP,  $\alpha 4$ ,  $\beta 2$ , and the ER marker dsRed-ER show a 1:1 correlation with ER marker and localization of  $\alpha 5$ -mEGFP (figure 3.4). Chronic or acute incubation with nicotine may rescue ER localization of  $\alpha 5$ -mEGFP and facilitate ER exit of  $\alpha 5$ -mEGFP containing receptors, possibly through a chaperoning-like mechanism. 4 h treatment of neurons transiently transfected with  $\alpha 5$ -mEGFP,  $\alpha 4$ ,  $\beta 2$ , and dsRed-ER with 1.0  $\mu\text{M}$  nicotine did not result in measurable changes in localization with ER marker. Other concentrations of nicotine were also investigated but no changes were observed.

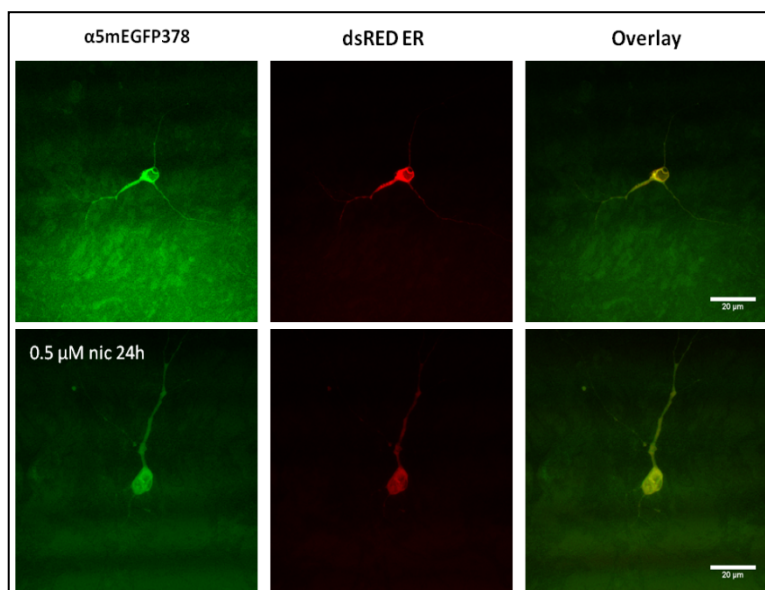


**Figure 3.4**

Representative images of mouse e17 cortical neurons expressing  $\alpha 5$ -mEGFP subunits with non-fluorescent  $\alpha 4$  and  $\beta 2$  subunits. Neurons were concurrently transfected with dsRED-ER, to delineate the endoplasmic reticulum.

Fluorescent expression of  $\alpha 5$ -mEGFP was characteristically low, and no obvious differences in co-localization with dsRED-ER were seen after 24 h incubation with 0.5  $\mu\text{M}$  nicotine.

24 h incubations were performed with 0.1  $\mu\text{M}$  nicotine, and the same result was seen. Parallel experiments conducted with the  $\alpha 5\text{D}398\text{N}$ -mEGFP mutant variant were performed for both 4 h and 24 h incubations, and no difference in co-localization with ER marker or phenotypic differences between  $\alpha 5$ -mEGFP and  $\alpha 5\text{D}398\text{N}$ -mEGFP were observed (figure 3.5).

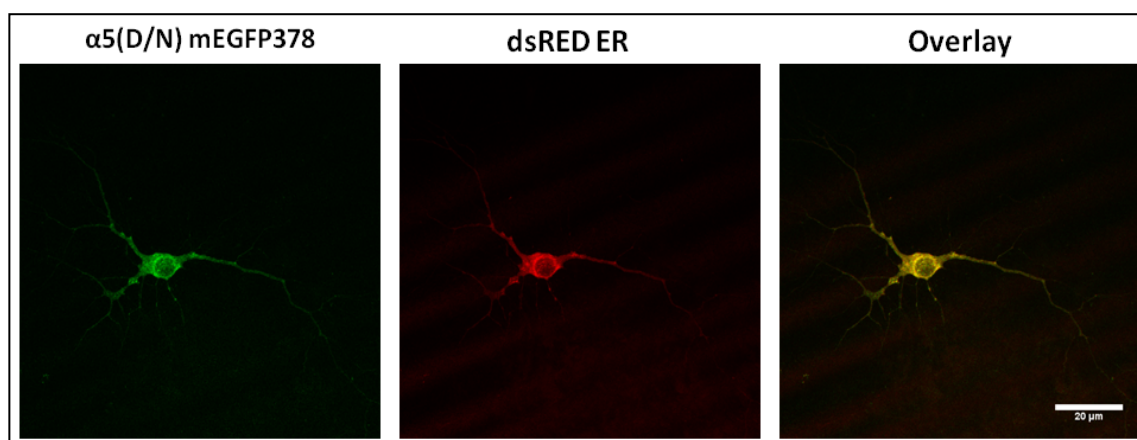


**Figure 3.5**

Representative images of  $\alpha 5D398N$ -mEGFP and ER marker dsRED-ER. Images were taken by scanning confocal microscope after excitation with 488 nm (mEGFP) or 561 nm (dsRED-ER) laser. Scale = 20 $\mu$ m. mEGFP images perfectly overlay with dsRED ER images, indicating that there is little expression of  $\alpha 5D398N$ -mEGFP outside the ER.

It is possible that differences in trafficking do occur, but the effects are subtle. Measurements of integrated membrane expression using Total Internal Reflection Fluorescence (TIRF) have been used to quantify differences in surface expression of  $\alpha 4\beta 2$  receptors after drug exposures [23]. Similar techniques could be applied to neurons expressing  $\alpha 4$  vs  $\alpha 5$  and/or  $\alpha 5D/N$  subunits. With the data reported here we are able to demonstrate expression of fluorescent  $\alpha 5$ -mEGFP and  $\alpha 5D/N$ -mEGFP constructs in mouse e17 cortical neurons. Optimized protocols for transfection, expression and imaging of these neurons are described in detail in appendix ii. Similar to results reported in chapter 1, even after optimization of imaging conditions, expression of fluorescent  $\alpha 5$  is consistently low compared to other fluorescent  $\alpha$  subunits. If we wish to study the endogenous behaviors of  $\alpha 5^*$  receptors, it is possible that other methods for fluorescent labeling must be used to improve visualization and ensure wild-type behavior of the labeled receptor.

From these data, we must conclude that there is little difference in trafficking of  $\alpha 4$ -mEGFP $\beta 2$  vs.  $\alpha 5$ -mEGFP $\alpha 4\beta 2$  receptors.  $\alpha 5$ -mEGFP $\alpha 4\beta 2$  receptors express much less efficiently, and  $\alpha 5$ -mEGFP fluorescence does not extend as far into the neuronal processes

as does  $\alpha 4$ -mEGFP, but this is most likely due to the large difference in expression level and not the result of differential trafficking. Incubation with  $1\mu\text{M}$  nicotine was not able to rescue ER localization of either the  $\alpha 5$ mEGFP $\alpha 4\beta 2$  or  $\alpha 5\text{D}/\text{NmEGFP}\alpha 4\beta 2$  receptor and no difference in expression or subcellular localization of these two receptors was seen. Taken together, these data suggest that the D398N mutation does not exert its influence over  $\alpha 5$ mEGFP $\alpha 4\beta 2$  by altering assembly or trafficking of the receptor.

## Chapter 4

### *Determination of nAChR stoichiometry using Normalized Försters Resonance Energy Transfer (NFRET)*

Försters resonance energy transfer (FRET) has become a technique widely used in the biological community to assay for protein-protein interactions. FRET describes the distance dependent, non radiative transfer of energy between a donor fluorophore in an excited state and an acceptor fluorophore in the ground state [40]. Donor fluorophores emit at wavelengths that overlap with the acceptor excitation spectrum. In biological applications these donor and acceptor molecules are frequently fluorescent protein variants of GFP. The Förster distance,  $R_0$ , is the distance at which energy transfer is 50% of the maximum, and for fluorescent proteins this distance tends to fall within a range of 40 – 60 Å. Within this distance, detection of a FRET signal is sufficient to indicate interaction between two independent FP labeled proteins [41-42].

FRET is sometimes called a “molecular ruler” as it can be used to directly measure the distances between donor and acceptor fluorophores [43]. This is especially useful when measuring conformational changes before and after ligand binding or during denaturation [44-45]. The distance between FRET donor and acceptor molecules can be simply calculated by equation 1. Where  $E_{FRET}$  is the efficiency of energy transfer,  $\tau_D$  is the decay rate of the donor in the absence of acceptor,  $R_0$ , is the distance at which energy transfer is 50% efficient, and  $r$  is the distance between donor and acceptor fluorophores.

$$(eq 1) \quad E_{FRET} = \frac{1}{\tau_D} \left( \frac{R_0}{r} \right)^6$$

This is a simplification from the greater equation given below for rate of FRET,  $k_T(r)$ , between a single donor, D, and acceptor, A, separated by a distance,  $r$ , where  $Q_D$  is the quantum yield of the donor,  $\kappa^2$  is the orientation factor for the donor and acceptor transition dipoles, and  $N$  is Avogadro's number.  $F_D(\lambda)$  is the corrected fluorescence intensity of the donor in the wavelength range  $\lambda$  to  $\lambda+\Delta\lambda$ , and  $\epsilon_A(\lambda)$  is the extinction coefficient of the acceptor at  $\lambda$ .  $n$  represents the refractive index of the medium and is assumed to be 1.4 for biological applications.

$$(eq\ 2) \quad k_T(r) = \frac{Q_D \kappa^2}{\tau_D r^6} \left( \frac{9000(\ln 10)}{128\pi^5 N n^4} \right) \int_0^\infty F_D(\lambda) \epsilon_A(\lambda) \lambda^4 d\lambda$$

Qualitatively, FRET can be used to determine whether two proteins come close enough together to form an interaction. If two FP labeled proteins are in close proximity, such that a FRET signal is detected, it can be implied that they are close enough to form direct interactions with each other. This approach has been applied to nAChRs. Drenan et al. demonstrated that  $\beta 3$  was incorporated into  $\alpha 6^*$  receptors by measuring FRET interactions between FP labeled  $\alpha 6$  and  $\beta 3$  subunits via donor recovery after photobleaching (DRAP) [22].

Within the nAChR pentamer, there are two possible distances between subunits. For instance, in the  $\alpha 6\alpha 4\beta 2\beta 3$  receptor  $\alpha 6$  subunits can be either adjacent, or non-adjacent to  $\beta 3$  subunits. When a receptor contains a single donor and acceptor FP pair there are two possible FRET outcomes that correspond to distance and position within the pentamer. Son et al. estimates that the distance ( $r$ ) between adjacent subunits,  $a$ , is approximately 5.2 nm and  $b$ , the diagonal distance between nonadjacent subunits is approximately 8.3 nm. Using

mEGFP and mCherry, and the donor and acceptor fluorophores,  $R_0 = 5.1$  nm, and equation 3 (a rearrangement of eq. 1)  $E_{FRET}$  is calculated to be 47% for adjacent FP and 5% for non-adjacent FP-labeled subunits. Therefore, it is theoretically possible to determine the position of an  $\alpha 6$ -mEGFP with respect to a  $\beta 3$ -mCherry subunit within an assembled pentamer.

$$(eq. 3) \quad E_{FRET} = \frac{\left(\frac{R_0}{r}\right)^6}{1 + \left(\frac{R_0}{r}\right)^6}$$

The  $\alpha 4\beta 2$  receptor presents additional challenges to interpretation of FRET data because it can be expressed in multiple stoichiometries of two or more of a single subunit subtype. When  $\alpha 4\beta 2$  receptors are expressed with FP labeled  $\alpha 4$  subunits, the  $\alpha 4$  may contain either a mEGFP or mCherry label. Possible label geometries are illustrated in figure 4.1. Nevertheless, from measurements of  $\alpha 4$  subunits labeled with the FRET donor/acceptor pair cyan fluorescent protein (CYP)/ yellow fluorescent protein (YFP), Son et al. proposed that the  $(\alpha 4)_2(\beta 2)_3$  and  $(\alpha 4)_3(\beta 2)_2$  stoichiometries can be differentiated using FRET [6].

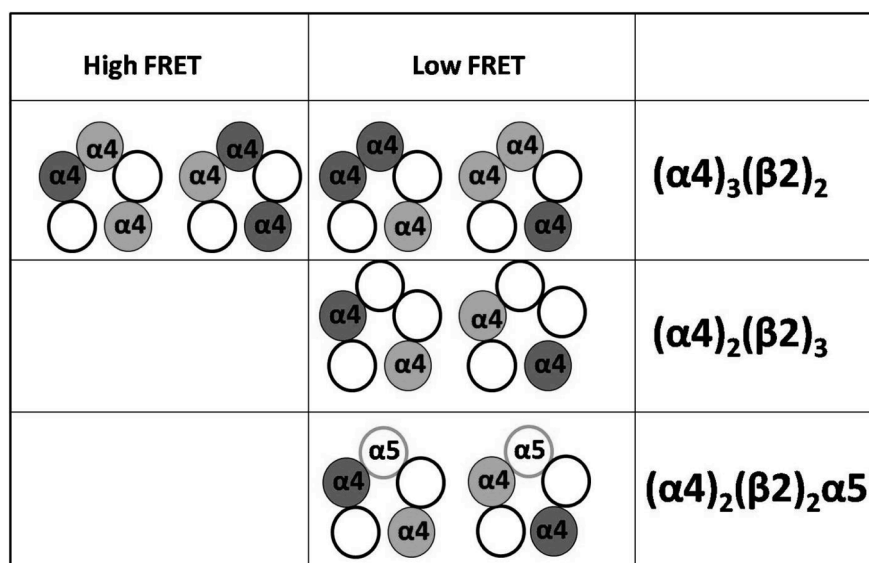


**Figure 4.1**  
Cartoon of  $\alpha 4\beta 2$  and  $\alpha 5\alpha 4\beta 2$  receptor pentamers, their stoichiometries and relative FRET values. Dark grey indicates a FRET donor, light grey indicates a FRET acceptor.

The calculation of  $E_{\text{FRET}}$  in the presence of multiple donor and acceptor molecules is complicated. In their analysis Son et al. make some necessary geometric assumptions:

1. “In a functional  $\alpha 4\beta 2$  receptor, there are at least two agonist binding sites at the  $\alpha$ - $\beta$  subunit interfaces (these are polarized, requiring particular faces of each subunit; see assumption 2 below). Therefore, in the  $(\alpha 4)_2(\beta 2)_3$  stoichiometry, the two  $\alpha 4$  subunits are nonadjacent, and in the  $(\alpha 4)_3(\beta 2)_2$  stoichiometry, the two  $\beta 2$  subunits are nonadjacent.
2. The  $\beta$  subunit is adjacent, in the clockwise direction, to the  $\alpha$  subunit.
3. Although the intracellular domain of the  $\alpha 4$  subunit has roughly twice as many amino acids as that of the  $\beta 2$  subunit, the fluorophores are positioned in an equilateral pentagonal structure.
4. All  $\alpha 4$  subunits are radially equivalent, and all  $\beta 2$  subunits are radially equivalent.
5. Because YFP (acceptor) and CFP (donor) differ by only nine amino acids, YFP- and CFP-tagged subunits are synthesized with equal efficiency and assemble

*randomly within receptor pentamers. The expected results are rather insensitive to departures from this assumption by even 2-fold.*

6. *Again, because YFP and CFP differ only subtly, the structure of an  $\alpha$ 4CFP subunit is the same as  $\alpha$ 4YFP; in addition, a  $\beta$ 2CFP subunit has the same structure as a  $\beta$ 2YFP subunit.*
7. *In a rigorous analysis, the dipole orientation factor  $\kappa^2$  differs between adjacent and nonadjacent subunit pairs. Analysis shows that, in general, the ratio  $\kappa^2$  (nonadjacent subunits)/ $\kappa^2$  (adjacent subunits) lies between 1 and 2; a full prediction requires knowledge of the dipole orientation, which we do not know. We assume that this ratio always equals 1.” [6]*

Using these assumptions, the difference in calculated  $E_{\text{FRET}}$  was dependent on the number of donor and acceptor subunits within the pentamer. Son et al. chose to examine the case in which only the  $\alpha$ 4 subunits are labeled with FPs. An assembled pentamer of  $(\alpha 4)_2(\beta 2)_3$  stoichiometry, contains only one possible arrangement of donor and acceptor FPs. The theoretical  $E_{\text{FRET}}$  calculated from equation 3 for a single mEGFP/mCherry pair in a non-adjacent arrangement is 5%.

The  $(\alpha 4)_3(\beta 2)_2$  stoichiometry, however, can assemble into four possible geometries (see figure 4.1). The measured  $E_{\text{FRET}}$  for a population of  $\alpha 4$ -mEGFP  $\alpha 4$ -mCherry $\beta 2$  receptors in an  $(\alpha 4)_3(\beta 2)_2$  stoichiometry becomes the weighted sum of the  $E_{\text{FRET}}$  for each geometry times the probability of the occurrence of the geometry. The theoretical  $E_{\text{FRET}}$  for each receptor conformation can be calculated using the equations below:

$$(eq. 4) \quad E_{\text{FRET}} (1 \text{ donor, nonadjacent to } 2 \text{ acceptors}) = \left( \frac{2 \left( \frac{R_0}{b} \right)^6}{1 + 2 \left( \frac{R_0}{b} \right)^6} \right)$$

$$\text{(eq. 5) } E_{\text{FRET}} \text{ (1 donor, adjacent and nonadjacent to 2 acceptors)} = \left( \frac{R_0^6 \left( \frac{1}{a^6} + \frac{1}{b^6} \right)}{1 + R_0^6 \left( \frac{1}{a^6} + \frac{1}{b^6} \right)} \right)$$

$$\text{(eq. 6) } E_{\text{FRET}} \text{ (2 donors, both nonadjacent to an acceptor)} = \left( \frac{\left( \frac{R_0}{b} \right)^6}{1 + \left( \frac{R_0}{b} \right)^6} \right)$$

$$\text{(eq. 7) } E_{\text{FRET}} \text{ (2 donors, each adjacent and nonadjacent to 1 acceptor)} = \frac{1}{2} \left( \frac{\left( \frac{R_0}{a} \right)^6}{1 + \left( \frac{R_0}{a} \right)^6} + \frac{\left( \frac{R_0}{b} \right)^6}{1 + \left( \frac{R_0}{b} \right)^6} \right)$$

Normalized Förster Resonance Energy Transfer (NFRET) has been used successfully to examine changes in between  $\alpha 4$  subunits ( $\alpha 4$ -EGFP and  $\alpha 4$ -mCherry) in cells transiently transfected with  $\alpha 4$  and  $\beta 2$  subunits and has provided clues to stoichiometric changes upon addition of pharmacological agents such as nicotine [46]. Detection of FRET is possible by measuring intensity of sensitized emission. Equation 8 describes the calculation of  $E_{\text{FRET}}$  based on intensity measurements.  $I_{\text{FRET}}$  is the intensity of the FRET signal,  $I_{\text{D}}$  is the measured fluorescent intensity of the donor fluorophore,  $BT_{\text{D}}$  is the bleed-through fluorescence detected in the acceptor channel after excitation of the donor.  $I_{\text{A}}$  is the fluorescent intensity of the acceptor fluorophore and  $BT_{\text{A}}$  is the bleed-through fluorescence of the acceptor.

$$\text{(eq. 8) } E_{\text{FRET}} = I_{\text{FRET}} - I_{\text{D}}BT_{\text{D}} - I_{\text{A}}BT_{\text{A}}$$

NFRET describes the measured  $E_{\text{FRET}}$  value after normalization with the square root of  $I_D$  and  $I_A$  (equation 9). This method is ideal for calculation of FRET within a multi-pixel image in which each image pixel may contain different numbers of FP labeled receptors and therefore display different fluorescence intensities [47].

$$(eq. 9) \quad E_{\text{NFRET}} = \frac{I_{\text{FRET}} - I_D B T_D - I_A B T_A}{\sqrt{I_D I_A}}$$

To examine the efficiency of unlabeled  $\alpha 5$  subunits into  $\alpha 4$ -mCherry $\alpha 4$ -mEGFP $\beta 2$  receptors, N2a cells were transiently transfected with DNA constructs of  $\alpha 4$ -mCherry,  $\alpha 4$ -mEGFP, and  $\beta 2$  subunits. Plasmid DNA constructs were transfected in a 1:1:1 ratio of  $\alpha 4$ -mCherry: $\alpha 4$ -mEGFP: $\beta 2$  to bias assembly of the  $(\alpha 4)_3(\beta 2)_2$  stoichiometry. 48 h post-transfection, cells were imaged at 37 °C on an Eclipse C1si laser-scanning confocal microscope with a 63 X, 1.4 numerical aperture, violet-corrected plan apochromatic oil objective and a multianode photomultiplier tube with 32 channels (Nikon Instruments Inc., Melville, NY). Images were linearly unmixed with the emission spectra of the donor and acceptor fluorophores using reference spectra. NFRET was measured using the PixFRET plugin for ImageJ [40, 47]. The calculated NFRET values per-cell were then plotted as average histograms and fitted to two Gaussian curves (see figure 4.2).

It was hypothesized that incorporation of unlabeled, wild-type  $\alpha 5$  constructs into  $\alpha 4$ -mCherry $\alpha 4$ -mEGFP $\beta 2$  parent receptors could be detected as a shift in calculated FRET values. Addition of an unlabeled  $\alpha 5$  subunit into an  $\alpha 4$ -mCherry $\alpha 4$ -mEGFP $\beta 2$  receptor population would lock the FP-labeled  $\alpha 4$  subunits geometries into a non adjacent position

and thus reduce the measured  $E_{\text{NFRET}}$  for the receptor population. N2a cells were transiently transfected with DNA constructs of  $\alpha 4$ -mCherry,  $\alpha 4$ -mEGFP,  $\beta 2$ wt and either  $\alpha 5$  or  $\beta 3$  subunits and compared to the  $\alpha 4$ -mCherry $\alpha 4$ -mEGFP $\beta 2$  control. However, no change in NFRET values or in the areas of the two Gaussians fit to the NFRET histogram was seen (figure 4.2).

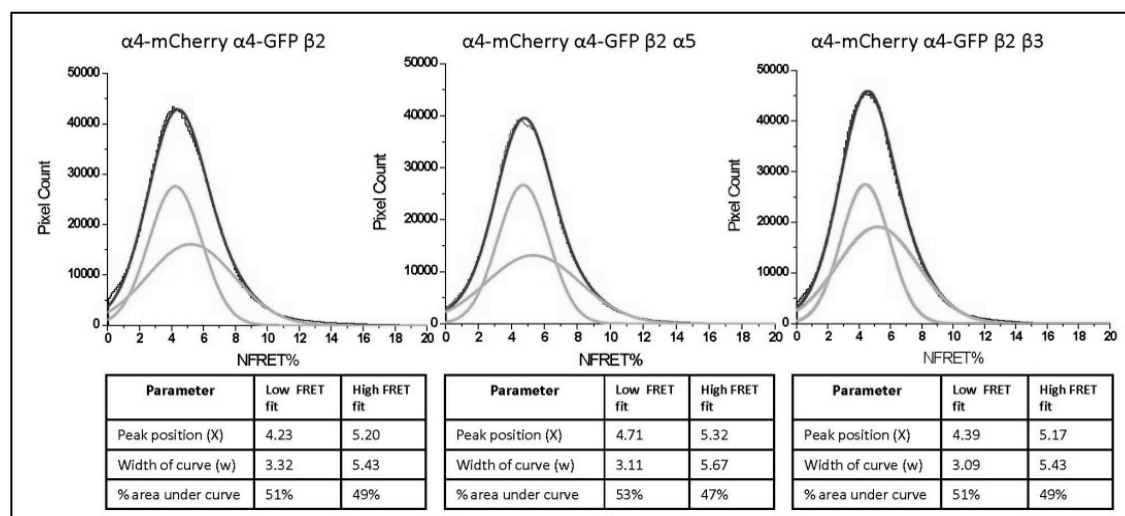


**Figure 4.2**

Sum histograms of NFRET calculated from images of N2a cells expressing fluorescent nAChRs. Each dark grey curve describes the sum NFRET calculated in 40 cells. Light grey curves describe Gaussian curves fit to the sum histogram. Properties of the fit Gaussians were intended to describe each sub population stoichiometry.

It was hypothesized that  $\alpha 4$ -mCherry $\alpha 4$ -mEGFP $\beta 2$  receptors may not incorporate accessory subunits as efficiently as other receptor subtypes.  $\alpha 3\beta 4$  are also known to incorporate  $\alpha 5$  and  $\beta 3$  accessory subunits [7]. NFRET was assayed in N2a cells expressing  $\alpha 3$ -mCherry $\alpha 3$ -mEGFP $\beta 4$ ,  $\alpha 3$ -mCherry $\alpha 3$ -mEGFP $\beta 4\alpha 5$ , or  $\alpha 3$ -mCherry $\alpha 3$ -mEGFP $\beta 4\beta 3$  subunits. A small shift was seen in the peak position of the second fit, corresponding to the “high-FRET” Gaussian component, but it was not found to be significant (figure 4.3).

It is possible that the incorporation of unlabeled  $\alpha 5$  subunits into  $\alpha 4\beta 2$  parent receptors is so inefficient that  $\alpha 4$ -mCherry $\alpha 4$ -mEGFP $\beta 2\alpha 5$  receptors do not represent a

large enough sub-set of the entire receptor population to change on measured NFRET values.

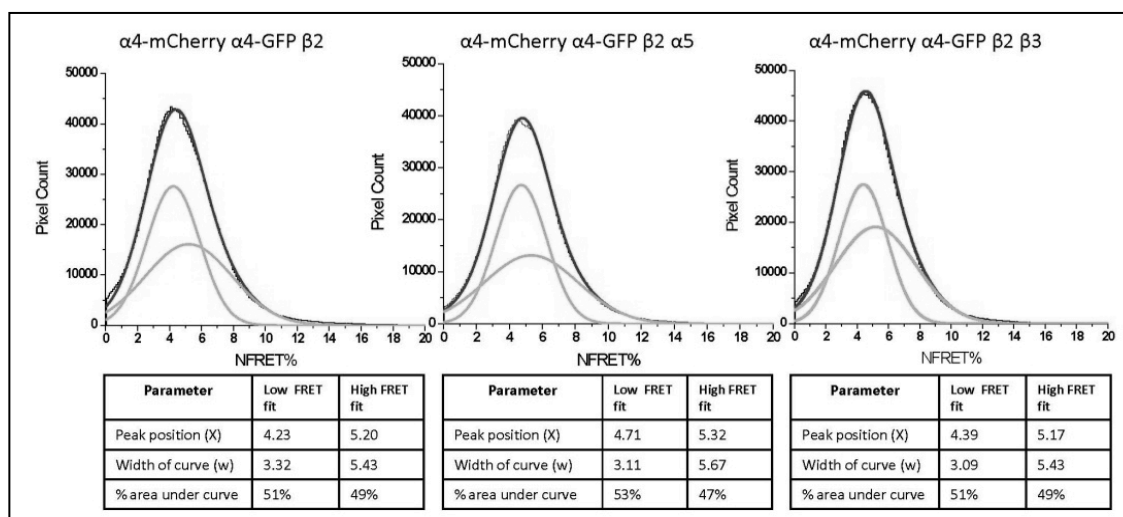


**Figure 4.3**

Sum histograms of NFRET calculated from images of N2a cells expressing fluorescent nAChRs. Each dark grey curve describes the sum NFRET calculated in 40 cells. Light grey curves describe Gaussian curves fit to the sum histogram. Properties of the fit Gaussians were intended to describe of each sub population stoichiometry.

In this case, a direct measurement of the  $\alpha 5^*$  receptor population would be preferable. Detection of interaction between  $\alpha 4$ -mCherry and  $\alpha 5$ -mEGFP could indicate subunit incorporation. NFRET measurements between  $\alpha 5$ -mEGFP378 and  $\alpha 4$ -mCherry were performed in HEK293 cells and yielded inconsistent NFRET signals. NFRET was detected in only 60% of cells imaged, and the peak NFRET value per cell showed high variability using the  $\alpha 5$ -mEGFP378 construct (figure 4.4).

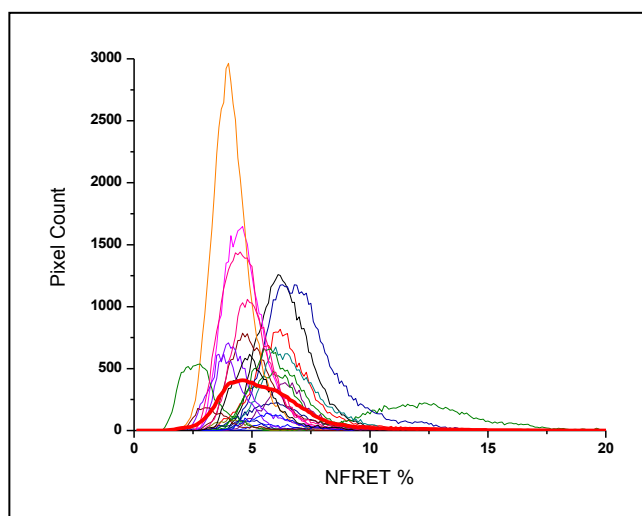


**Figure 4.4**

Same as figure 1.4

23 individual histograms of NFRET positive pixels in images of HEK293 cells expressing  $\alpha 5$ -mEGFP378,  $\alpha 4$ -mCherry, and  $\beta 2$  subunits. Bolded histogram describes the average of all 23 cells.

Distribution of individual cell histograms show significant variability in NFRET calculated for each individual cell. Average peak appears to be near 5% NFRET.

Inconsistency in NFRET data led to the hypothesis that NFRET was not measuring fully-assembled nAChR pentamers but that NFRET measurements were dominated by intracellular sub-assemblies of dimers, trimers, and tetramers. To test this hypothesis, a series of transfections was performed with  $\alpha 4$  or  $\alpha 5$  subunits in the absence of  $\beta 2$ . Without the  $\beta 2$  subunit it is impossible for a fully formed pentamer to assemble. Figure 4.5 shows that NFRET signals are not indistinguishable by eye when N2a cells are transfected with  $\alpha 4$ -mCherry and  $\alpha 4$ -mEGFP, or  $\alpha 4$ -mCherry  $\alpha 4$ -mEGFP and  $\beta 2$  subunits. However, no statistical difference was found after a two-sample independent t-test between the total FRET positive pixels of these two cell populations ( $p = 0.50$ ) (see also appendix iii).

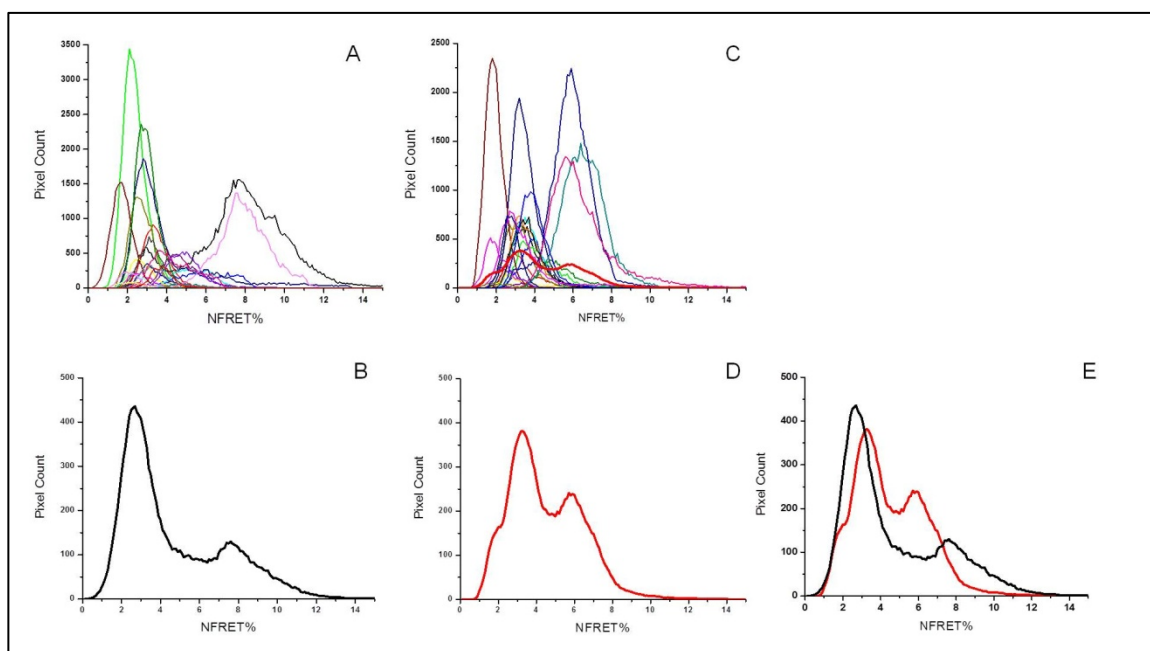


**Figure 4.5**

A. Raw fit histograms of NFRET from  $\geq 40$  N2a cells expressing  $\alpha 4$ -mEGFP and  $\alpha 4$ -mCherry without  $\beta 2$ . Bolded line indicates the average of the raw fits.

B. Average fit histogram of cells described in A.

C. Raw fit histograms of NFRET from  $\geq 40$  N2a cells expressing  $\alpha 4$ -mEGFP and  $\alpha 4$ -mCherry and  $\beta 2$ . Bolded line indicates the average of the raw fits.

D. Average fit histogram of cells described in C.

E. Overlay of average fit histograms for NFRET calculations in cells that do have the ability to form complete  $\alpha 4\beta 2$  pentamers (C and D, light grey line) and cannot form complete pentamers (A and B, dark grey line).

NFRET measurements were performed on N2a cells expressing either  $\alpha 4$ -mCherry and  $\alpha 5$ -mEGFP, or  $\alpha 4$ -mCherry  $\alpha 5$ -mEGFP and  $\beta 2$  subunits with similar results. Figure 4.6 shows an overlay of average NFRET histograms for both the  $\alpha 5$ -mEGFP $\alpha 4$ -mCherry and  $\alpha 5$ -mEGFP $\alpha 4$ -mCherry $\beta 2$  conditions. No statistical difference was found after a two-sample independent t-test between the total FRET-positive pixels in the  $\alpha 5$ -mEGFP $\alpha 4$ -mCherry vs.  $\alpha 5$ -mEGFP $\alpha 4$ -mCherry $\beta 2$  cell populations ( $p = 0.90$ ) or of mean FRET values of  $\alpha 5$ -mEGFP $\alpha 4$ -mCherry expressing cells vs.  $\alpha 5$ -mEGFP $\alpha 4$ -mCherry $\beta 2$  expressing cells ( $p = 0.35$ ) (appendix iii).

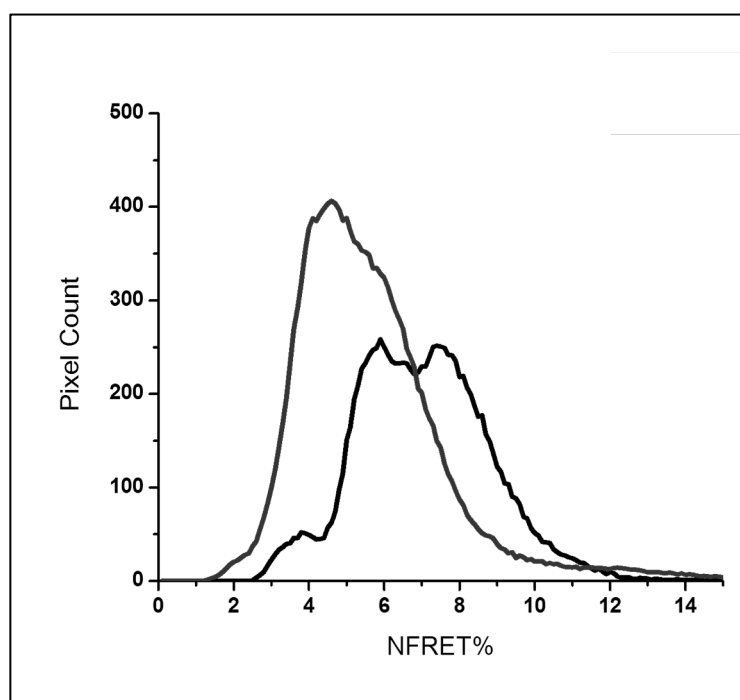


Figure 4.6

Overlay of average fit NFRET histograms from  $\geq 40$  N2a cells expressing  $\alpha 5$ -mEGFP and  $\alpha 4$ -mCherry without  $\beta 2$  (dark grey line), or with  $\beta 2$  (light grey line).

No statistical difference was seen in the two populations leading to the conclusion that NFRET may not be a reflective measure of receptor stoichiometry, but instead may indicate number and composition of intracellular receptor sub-assemblies.

Taken together, these data suggest that the measured NFRET is not reflective of assembled pentameric receptor complexes, but are primarily dimers or other incomplete assemblies. We conclude that NFRET signals are disproportionately influenced by unpaired subunits, possibly in intracellular compartments, and cast doubt on the eligibility of this

technique for use in stoichiometric determination of assembled nAChR receptor complexes as proposed by Son et al., and Srinivasan et al. [6, 23]. Using NFRET we have successfully demonstrated that  $\alpha 5$ -mEGFP and  $\alpha 4$ -mCherry do interact within the cell. This may indicate that  $\alpha 5$ -mEGFP assembles with  $\alpha 4$ -mCherry and  $\beta 2$  to form a complete receptor pentamer, but no assumptions can be made about stoichiometry using this approach.

## Chapter 5

### *TIRF-FLIM-FRET Engineering a Technique for High Resolution Detection of nAChR Composition and Stoichiometry*

nAChR subtypes are selectively expressed in distinct brain regions and cell types based on their subunit composition [7]. Subtle differences in receptor stoichiometry can influence receptor pharmacology and disease states [1, 4, 13, 48]. For example,  $\alpha 6^*$  receptors are an important neuronal nAChR subtype for nicotine reward, and these receptors can assemble with multiple stoichiometries and composition.  $\alpha 6\alpha 4\beta 2$ ,  $\alpha 6\alpha 4\beta 3\beta 2$ ,  $\alpha 6\beta 2$ , and  $\alpha 6\beta 3\beta 2$  are all possible  $\alpha 6^*$  subtypes [7, 11, 49]. These subtypes are differentially expressed in brain regions important for dependence, mood, and Parkinson's disease. In the interest of drug design, it would be beneficial to not only be able to identify which subunits are present in an expressed receptor but also to determine the position within the nAChR pentamer each subunit occupies. This information would be invaluable for development of future pharmacological agents selective for each receptor composition and stoichiometry.

Determination of nAChR stoichiometry was attempted using FRET between FP labeled nAChR subunits [6, 21-23, 26]. However, the work presented in chapter 4 strongly suggests that FRET measurements performed using sensitized emission are not a direct measurement of assembled receptor stoichiometry. Other fluorescence based methods have been applied to stoichiometric determination. Single molecule photo bleaching experiments successfully differentiated both stoichiometries of the  $\alpha 4\beta 2$  receptor through the counting of individual bleaching steps of mEGFP molecules fused to the nAChR subunits [50]. Additionally, donor recovery after photo bleaching (DRAP) measured FRET between

nAChR subunits for determination of receptor composition [21-22]. None of these methods have the sensitivity to determine the position of a donor with respect to an acceptor fluorophore within the pentamer, and interpretation of data is often complicated by background fluorescence from unpaired, unassembled subunits within the cell.

Fluorescence Lifetime Imaging Microscopy (FLIM) offers higher sensitivity FRET measurements over the sensitized emission techniques described in chapter 4. Sensitized emission relies on detection of both donor and acceptor intensity for calculation of  $E_{\text{FRET}}$ . FRET detection by FLIM is dependent only on changes in the lifetime of the donor fluorophore and is therefore a more direct measurement. By definition, FRET is an alternative path of fluorescent decay for an excited donor molecule to an acceptor molecule in the ground state. This non-radiative transfer of energy reduces the occupancy time (or lifetime) of the donor molecule in the excited state and this shorting of fluorescence lifetime can be measured and quantified. The efficiency of FRET ( $E_{\text{FRET}}$ ) can be calculated for donor and acceptor molecules of single exponential decay and fixed distance using equation 10, where  $\tau_D$  is the fluorescent lifetime of the donor fluorophore, and  $\tau_{DA}$  is the lifetime of the donor in the presence of a FRET acceptor [40, 51].

$$(eq. 10) \quad E_{\text{FRET}} = 1 - \frac{\tau_{DA}}{\tau_D}$$

The singular dependence on donor lifetime for FRET measurement via FLIM not only eliminates the problem of background and bleed-through fluorescence from unpaired subunits, but generation of a time-correlated single-photon-counting (TCSPC) histogram yields additional information about the percentage of donor fluorophores experiencing

FRET [52-53]. TCSPC is the most common detection method for FLIM, and it allows calculation of fluorescent lifetimes by measuring the time difference between a single laser pulse and the detection of an emitted photon by a photo-multiplier tube (PMT) or other detection device. These detection events are then binned and plotted across time points and the resulting histogram is the fit to one or more exponential decay curves from which fluorescence lifetimes ( $\tau$ ) can be extracted [52].

Preliminary experiments measuring FRET by FLIM using TCSPC and confocal microscopy led to challenges to data interpretation that were similar to those seen with other methods using confocal microscopy: FRET signals were homogenous for all experimental conditions and it was impossible to determine differences in receptor composition (Richards and Sedak 2011, unpublished data). Use of FLIM eliminates the problem of bleed-through fluorescence from directly excited acceptor molecules, but it is unable to distinguish fully assembled pentamers from sub-assemblies of nAChR subunits such as dimers, trimers, and tetramers in intracellular compartments visible in a confocal image. We hypothesized that the homogeneity in FRET calculations could be due to these partially assembled subunit complexes that could comprise the majority of the  $\tau_{DA}$  component.

Only assembled, pentameric receptors are trafficked to the surface of the cell; therefore, Total Internal Reflection Fluorescence (TIRF) microscopy can be used to isolate assembled receptors for visualization. TIRF microscopy exploits the evanescent wave that occurs when the incident beam of light is totally internally reflected at a glass-water interface [54]. The wave penetrates into the cell with an intensity that decays exponentially such that only fluorophores within  $\leq 200$  nm of the cell surface are excited. TIRF has been

used to selectively excite populations of fully assembled, pentameric nAChRs at the plasma membrane for studies on trafficking and upregulation [23]. TIRF and FLIM have not previously been performed in concert. By combining these techniques (TIRF-FLIM) we have engineered the capability to selectively measure FRET interactions within nAChR pentamers at or near the cell surface for high resolution detection of composition and stoichiometry.

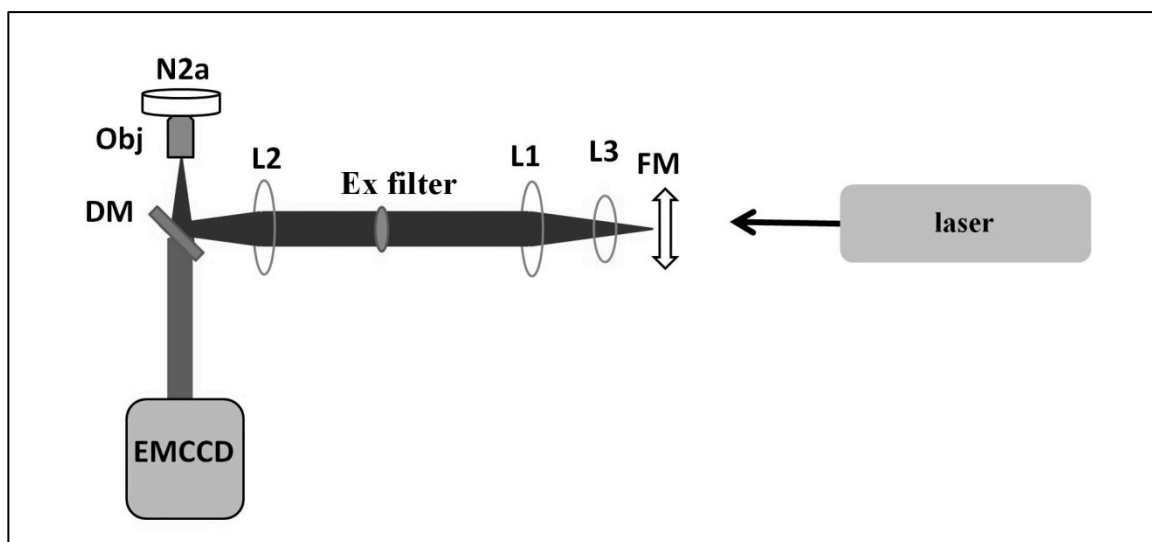


**Figure 5.1A**

Schematic of a conventional TIRF microscope.

FM = focal mirror, L = lens, Ex filter = Excitation filter, Obj = 100X 1.45 NA oil-immersion objective lens, N2a indicate the sample dish containing N2a cells, DM = dichroic mirror, EMCCD = Olympus CCD camera.

Adaptation of an existing TIRF microscope for TCSPC FLIM detection required several modifications. Figure 5.1A illustrates an Olympus IX81 inverted microscope with TIRF capability [50]. A 488nm picosecond pulsed diode laser (PDL 800-D, PicoQuant GmbH) was mounted to the back port of the microscope and a diverter was added to the output to re-direct light from the ccd camera to a single photon counting board (PMT) (SPCM-AQR SPAD, Perkin Elmer). The PMT detector was connected to a TCSPC module and event timer (PicoHarp 300, PicoQuant GmbH) and a separate windows PC loaded with PicoHarp 2.0 software (Figure 5.1B).

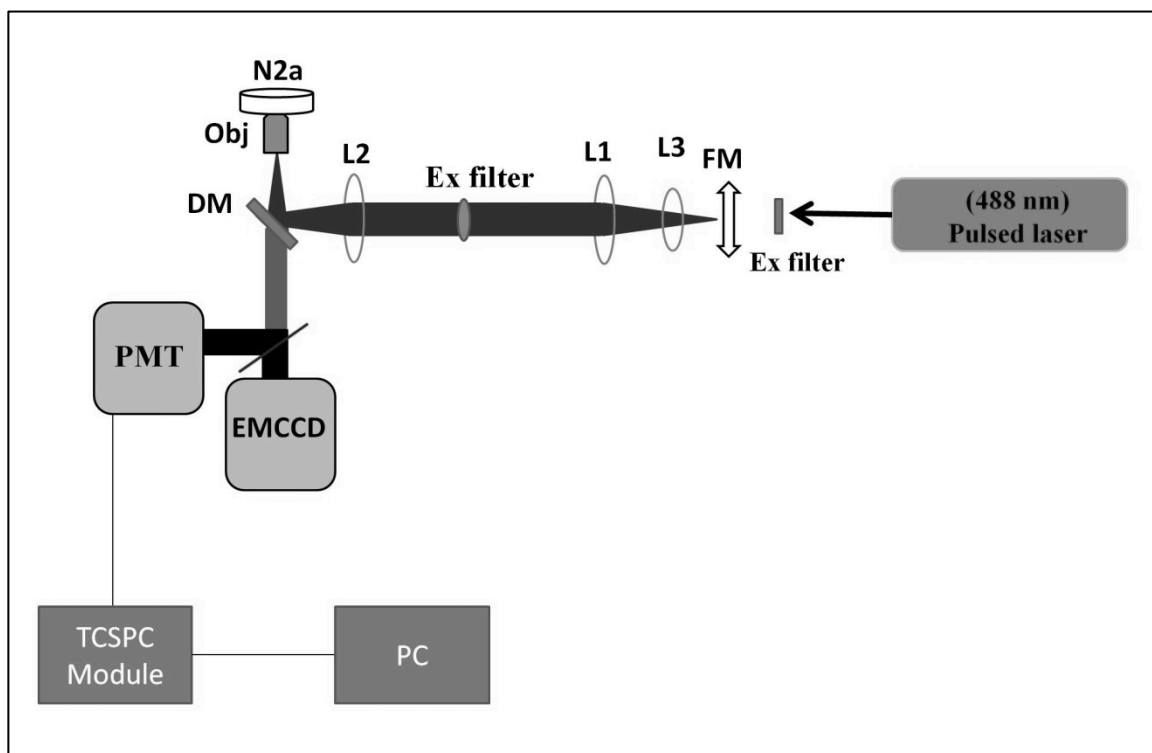


**Figure 5.1B**

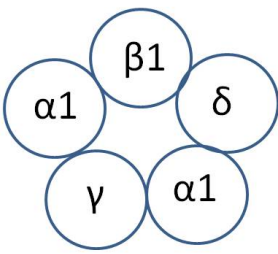
Schematic of modifications made to conventional TIRF microscope for addition of FLIM capability. FM = focal mirror, L = lens, Ex filter = Excitation filter, Obj = 100X, 1.45 NA oil-immersion objective lens, N2a indicate the sample dish containing N2a cells, DM = dichroic mirror, EMCCD = Olympus CCD camera, PMT = photo multiplier tube. TCSPC Module = time correlated single photon counting module with single event timer, PC = personal windows computer with PicoHarp 2.0 software.

The mouse muscle nAChR was selected as the model receptor for technique validation because, unlike the neuronal nAChRs, it has a fixed stoichiometric composition of  $(\alpha 1)_2\beta 1\gamma\delta$  [2, 55]. The fixed nature of the muscle nAChR stoichiometry and composition allows measurement of FRET between each geometric relationship within the pentamer. By varying which subunits are fluorescently labeled in expressed receptors, we are able to straightforwardly measure the  $E_{\text{FRET}}$  values for single-adjacent and single non-adjacent FRET pairs, as well as each multiple donor and acceptor permutation (see figure 5.2). Fluorescent labels were introduced into mouse muscle subunits following methods well described by Lester et al. [6, 21-23].

Table 3 lists the constructed fluorescent subunits. Preliminary FLIM experiments performed using confocal microscopy revealed an inexplicable second lifetime in mEGFP control measurements (Richards and Sadek 2011, unpublished data). However, mYFP consistently displayed a single  $\sim 2.9$  ns lifetime. mYFP was therefore selected as the donor fluorophore for TIRF-FLIM experiments with mCherry as the acceptor.

**Table 3**

Subunit	Fluorescent Protein	Subunit	Fluorescent Protein
$\alpha$	none	$\alpha$	mGFP
$\alpha$	mYFP	$\alpha$	mYFP Y66C
$\alpha$	mCherry	$\alpha$	mYFP Y145W
$\beta$	none	$\beta$	mGFP
$\beta$	mYFP	$\beta$	mYFP Y66C
$\beta$	mCherry	$\beta$	mYFP Y145W
$\gamma$	none	$\delta$	mGFP
$\gamma$	mYFP	$\delta$	mYFP Y66C
$\gamma$	mCherry	$\delta$	mYFP Y145W
$\delta$	none	$\gamma$	mGFP
$\delta$	mYFP	$\gamma$	mYFP Y66C
$\delta$	mCherry	$\gamma$	mYFP Y145W

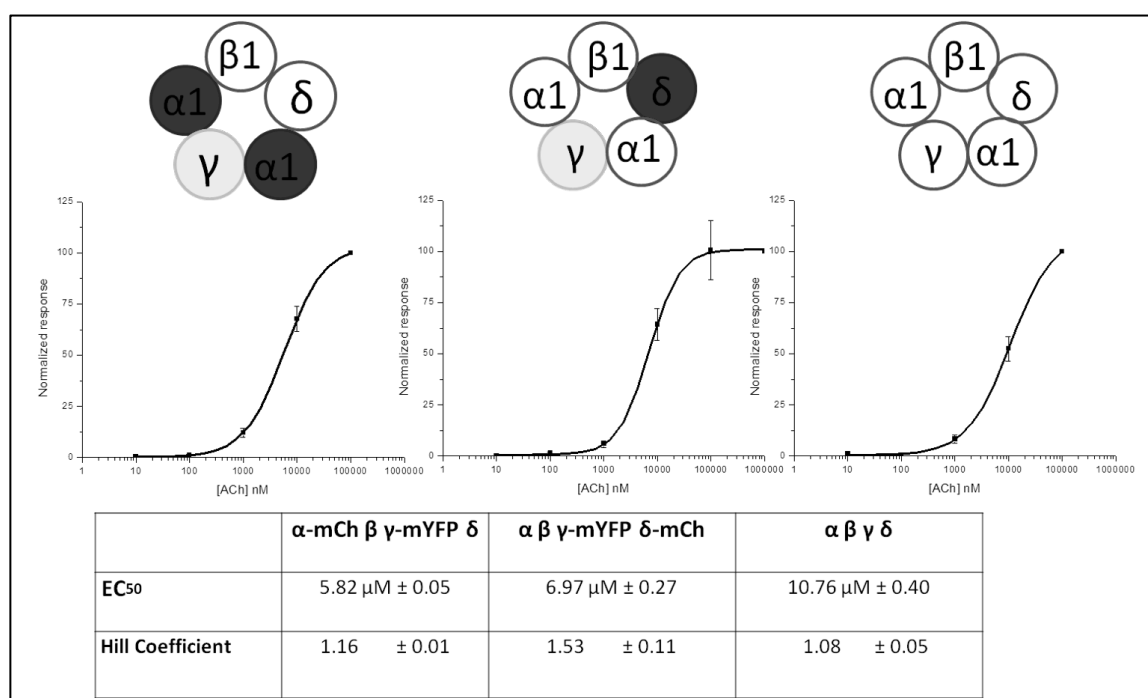


The diagram shows a protein complex consisting of five subunits arranged in a pentagonal pattern. The subunits are labeled as follows:  $\beta 1$  at the top,  $\alpha 1$  on the left,  $\delta$  on the right,  $\gamma$  at the bottom-left, and  $\alpha 1$  at the bottom-right.

$E_{\text{FRET}}$ theoretical	77%	36%	36%	9%	9%	63%	63%
$E_{\text{FRET}}$ measured	$71.49 \pm .55\%$	$71.93 \pm .43\%$	$70.26 \pm .60\%$	$75.47 \pm .64\%$	$73.15 \pm .44\%$	$70.24 \pm 1.1\%$	$72.47 \pm .47\%$
FRET Fraction	$36.07 \pm 1.1\%$	$28.70 \pm 1.0\%$	$28.91 \pm 2.6\%$	$16.53 \pm 1.5\%$	$18.32 \pm 1.2\%$	$21.46 \pm 1.2\%$	$21.76 \pm 2.1\%$

**Figure 5.2**

Illustration of some fluorescent muscle receptor stoichiometries and their measured  $E_{\text{FRET}}$  values. Dark grey fill indicate FRET acceptor (mCherry) and light grey fill indicates FRET donor 9mYFP). No fill indicates no FP tag is present on the subunit. FRET fraction refers to the percentage of donor fluorophores that had shortened lifetimes due to FRET.

**Figure 5.3**

Acetylcholine dose response curves for muscle nAChRs expressed in differentiated N2a cells 48 h post transfection. Cartoon of receptor pentamer indicates receptor type. Dark grey fill indicates FRET acceptor (mCherry), light grey fill indicates FRET donor (mYFP), no fill indicates no FP label was present on the subunit.

Fluorescent subunits were verified for function using the same methods described in chapter 1. Electrophysiological recordings were performed by Tim Indersmitten on differentiated N2a cells transiently transfected with FP- or non FP-tagged muscle nAChR

subunits. Figure 5.3 displays some of the recorded dose response curves and  $EC_{50}$  values for these receptors. Measured  $EC_{50}$  were two-fold higher than values reported from *Xenopus* oocytes but these variations could be attributed to the differences in receptor expression system [56]. When fluorescent nAChR subunits were transfected without all the necessary subunits, no measureable currents were seen.

N2a cells were transiently transfected in growth media under serum-starved conditions to encourage differentiation (appendix ii) [57]. Differentiated N2a cells have extended processes and increased adhesion to the glass coverslip. This increased surface area contributes to an improved TIRF signal over non-differentiated N2a cells. Cells were imaged 24 h after transfection in  $CO_2$  buffering Leibovitz media without phenol-Red. Temperature was maintained at 37 °C during imaging using an incubator installed on the microscope stage and a heating coil that warmed the objective itself to 37 °C. Samples were excited with 488 nm pulsed laser illumination, and data was collected using a PMT with TCSPC module.

Single cells were imaged at a time. One disadvantage of lifetime imaging with our adapted TIRF microscope is the loss of spacial resolution achieved with scanning confocal. All photons from the excited sample are collected by the PMT as if from a single pixel. An adjustable aperture was used to restrict illumination of the sample to only the cell of interest to avoid contaminant photons from other cells in the field of view. Laser intensity was adjusted to achieve a photon detection rate of approximately 1000 kCounts/s. Sample data was collected for a minimum of  $2 \times 10^3$  total photons/cell to insure sufficient points for reliable exponential fits of the TCSPC histogram. PicoQuant GmbH proprietary SymPhoTime software was used for all data records and analysis.

Control experiments performed with single mYFP/mCherry FRET pairs revealed inconsistencies in measured mYFP lifetime. In the absence of mCherry the measured lifetime ( $\tau_D$ ) of mYFP maintained an average of 2.9 ns, a number consistent with literature report [58]. However, when mCherry was also present the measured  $\tau_D$  was artificially shortened and exhibited unusual variability (see figure 5.4). This inconsistency complicated determination of  $\tau_{DA}$  and perhaps unsurprisingly,  $E_{FRET}$  calculated from these fits did not track with theoretical values (see figure 5.2).

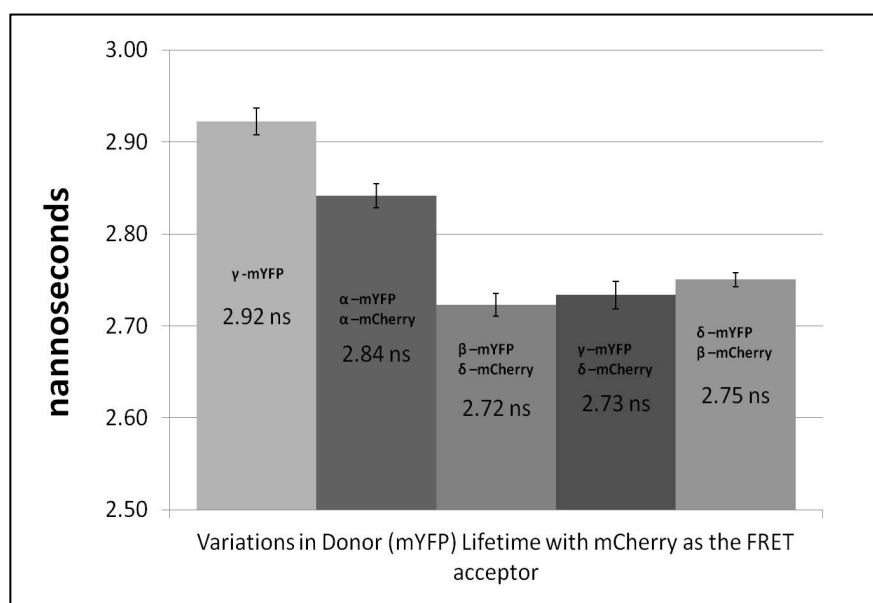


**Figure 5.4**

Bar graph describing variation in calculated non-FRET lifetimes of mYFP donors in the presence of different mCherry acceptors.

It is expected that calculated non-FRET donor lifetime should not change regardless of the presence of a FRET acceptor. This unexpected variability complicated lifetime fits and  $E_{FRET}$  calculations.

Significant variability in mYFP lifetime in the presence of mCherry led to investigation into the fluorescent properties of mCherry. It was discovered that mCherry exists in two possible brightness states that correspond to two distinct fluorescence lifetimes [59]. When mCherry is used as a FRET acceptor the energy transfer rate from the donor is different for each brightness state, and equation 10 cannot be applied for calculation of  $E_{FRET}$ . We

concluded that mCherry is not an ideal FRET acceptor for FLIM experiments, and a new FRET pair was selected.

mEGFP is the ideal FRET donor for our system. The pulse laser excites at 488nm, a wavelength closer to the absorption maxima of mEGFP (485 nm) than to mYFP (514 nm). Due to lack of success achieving a single exponential fit for a pure population of mEGFP when measured via confocal microscope, mEGFP was initially disregarded as a potential FRET donor. Indeed, TIRF-FLIM measurements of mEGFP lifetime also yielded a two exponential decay behavior. Acting on a hunch, we hypothesized that the fast, second component contaminant in the mEGFP decay curve could be photons from the laser itself. Addition of a direct excitation filter (474/21) just after the laser in-port and a more stringent emission filter (520/34) eliminated the second lifetime component. With these modifications, a single component decay curve ( $\tau = 2.8$  ns) was achieved for a pure population of mEGFP labeled nAChR subunits.

This advance allowed us to proceed using the mYFP as the FRET acceptor. The large blue-shifted tail of the mYFP absorbance spectra does not make mYFP an ideal acceptor for traditional FRET applications because of direct excitation of mYFP by the 488 nm laser. Direct excitation depopulates the fluorescent acceptor molecules in the ground state that can be excited through FRET by mEGFP. This fluorescence bleed through contaminates detection of FRET by sensitized emission (equation 8 chapter 4). FLIM only measures behavior of the donor fluorophore and therefore we are not concerned with the emission of acceptor fluorescence. mYFP can therefore be used as a FRET acceptor for FLIM.

Besides the assumption of single lifetime decays, equation 10 requires that the donor and acceptor fluorophores be separated by a fixed distance. The FP labels reside in the long flexible M3-M4 loop region of the nAChR subunits. It is possible that the flexibility of these unstructured regions allows enough movement of the fluorophores that this condition is not satisfied. Introduction of steric constraints in the intracellular loop regions may restrict movement of the FP labels and improve  $E_{\text{FRET}}$  calculations. A dark XFP variant would be useful for this purpose because such a label would retain identical properties to the mEGFP and mYFP proteins without addition of another fluorescent species to the experimental system.

mYFP-Y66C is a mutant variant of YFP that is unable to form a functional chromophore due to cysteine substitution at a crucial Y66 residue. Therefore, mYFP-Y66C has the same properties of mYFP but is unable to absorb or emit fluorescence [60]. Using mYFP-Y66C as a “place-holder” label on subunits that are not labeled with a FRET donor or FRET acceptor allows us to apply the distance assumptions proposed by Son et al. [6]. We hypothesize that expression of mouse muscle nAChRs containing mEGFP, mYFP, or mYFP-Y66C labels on subunits in fixed relationships within the pentamer will satisfy the system requirements as dictated by equation 10.

N2a cells were transfected with mouse muscle nAChR subunits, each bearing a mEGFP, mYFP, or mYFP-Y66C fluorescent label. Visualization with TIRF microscopy 24h post-transfection revealed little or no receptor expression on the plasma membrane. Pseudo-TIRF images of differentiated N2a cells expressing muscle nAChR pentamers illustrate the challenges to expressing a fully labeled receptor. It appears that when all five

subunits contain a FP label, receptor expression on the plasma membrane is severely impaired (figure 5.5).

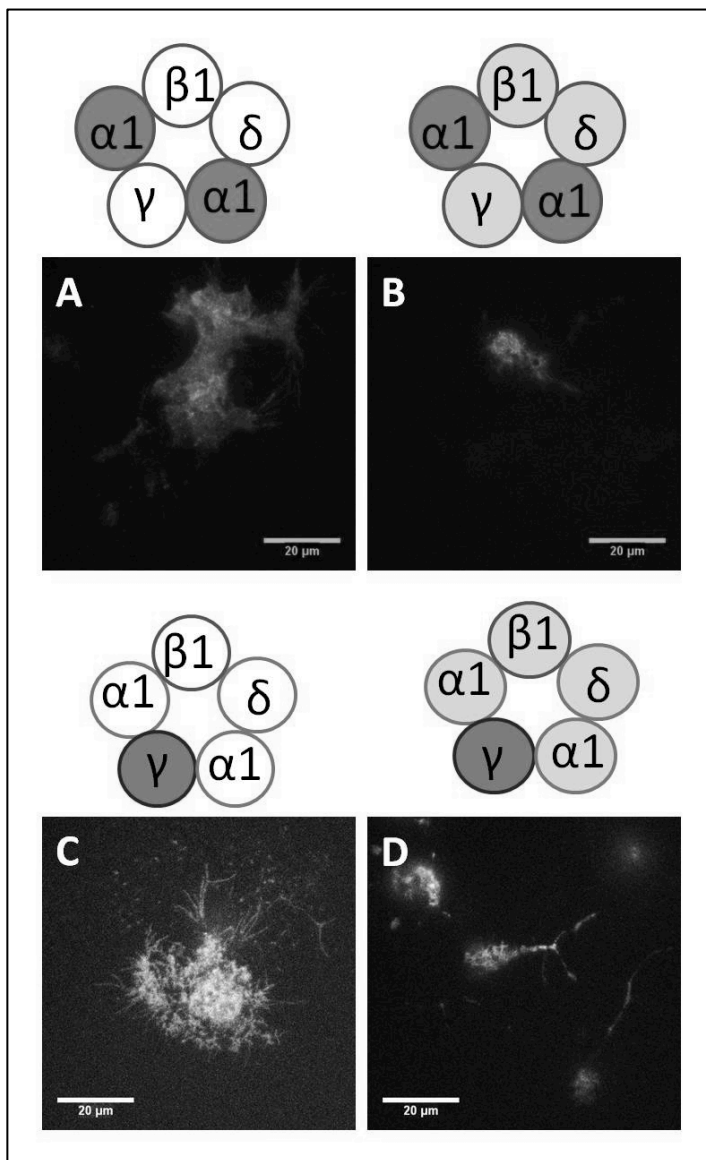


**Figure 5.5**

Example TIRF images of differentiated N2a cells expressing fluorescent nAChRs. Images were taken 48 h post transfection after excitation at 488 nm. Dark grey fill indicates fluorescent subunits. Light grey fill indicates subunits with mYFP-Y66C labels.

A.  $\alpha 1$ -mEGFP $\beta 1\gamma\delta$  shows strong expression and clear membrane fluorescence

B.  $\alpha 1$ -mEGFP( $\beta 1\gamma\delta$ ) -mYFP-Y66C shows only intracellular expression and little to no membrane fluorescence.

C.  $\alpha 1\beta 1\gamma$ -mYFP $\delta$  shows strong surface expression and clear membrane fluorescence.

D.  $\gamma$ -mYFP( $\alpha 1\beta 1\delta$ )-mYFP-Y66C shows only intracellular expression and little to no membrane fluorescence.

These data indicate that fully labeled muscle nAChRs do not traffic to the plasma membrane.

Fully labeled neuronal nAChRs such as  $\alpha 4$ -mEGFP $\beta 2$ -mCherry have successfully been expressed in N2a cells and imaged using TIRF [23, 50]. It is unclear why expression of the labeled muscle nAChR was unsuccessful. A possible hypothesis is that the FP labels obscured protein sequences in the M3-M4 loop that are important for receptor trafficking.

Trafficking motifs in the neuronal beta subunits are important for membrane expression [23]. We examined sequences of muscle  $\beta 1$ , and the neuronal  $\beta 2$  and  $\beta 4$  M3-M4 loops to determine if FP interference with trafficking signals could be the cause of aberrant expression of fully labeled muscle nAChR (figure 5.6). Figure 5.6 displays the alignment of M3-M4 loop sequences for  $\beta 1$ ,  $\beta 2$ , and  $\beta 4$ . No trafficking motifs were identified in the  $\beta 1$  sequence. It is possible that the muscle receptors contain as yet unidentified motifs important for vesicular transport of assembled receptors to the plasma membrane.

mouse $\beta 2$	KVVFLEKLP <b>TLLEFL</b> QQPRHRCARQRLRL <b>RRRQR</b> EREGAGTLFFREGPAAD
mouse $\beta 4$	KECFLHKLPT <b>FLFM</b> KRPGLEVSPARVPHSSQLHLTTAEATSTTSALGPSSP
mouse muscle $\beta 1$	RQIFIHKLPPYLGLKRPKPERDQLPEPHHS-LSPRSGWGRGTDEYFIRKP

**Figure 5.6**

Alignment of mouse beta M3-M4 loops. Mouse  $\beta 2$  contains both a forward trafficking LFM and an ER retention RRQR sequence (bold), and mouse  $\beta 4$  contains only an IFM sequence (bold). No trafficking sequences were identified in the mouse muscle  $\beta 1$  M3-M4 loop.

It is obvious that optimization of labeled muscle nAChR expression must occur before FLIM-FRET experiments are attempted. Approaches to improving surface expression of the labeled receptors include movement of the FP insertion location within the M3-M4 loop, extension of the flanking linker sequence to allow space for interaction with protein components of the vesicular transport system, and expression in a non-neuronal cell type. Complete analysis of M3-M4 loop sequences of the muscle nAChR subunits was performed before insertion of FP labels and care was taken to avoid any motifs known to be important for processing and transport of the receptor. It is possible that these subunits contain as yet unidentified sequences that perform this signaling function. If so, construction of additional fluorescent muscle subunits with FP inserted into alternative M3-M4 loop may avoid disruption of these unidentified sequences and restore proper trafficking and function to the labeled receptor.

It may also be the case that the FP insertion does not disrupt an unknown trafficking signal but that the presence of a FP label on all five subunits obscures access of trafficking proteins to these signal sequences. If this is the case, significant extension of the G-A-G and A-G-A linkers flanking the inserted FP gene may enable proper identification of trafficking motifs and successful membrane expression. Lastly, it is possible that heterologous expression of muscle type nAChRs is more efficient in muscle derived cell lines. Differentiated N2a cells were selected for use in these experiments due to the large surface area of the cell in contact with the imaging cover slip. This is ideal for TIRF imaging but may not be optimal for muscle receptor expression. A cell type derived from a muscle lineage may be more successful at expression of muscle nAChRs. c2c12 cells are derived from mouse muscle myoblasts and can express fluorescently labeled nAChRs. These cells may be a more amenable expression system for fully labeled muscle nAChRs.

In this chapter, we have described unique fluorescent protein constructs for the study of mouse muscle nAChRs and necessary modifications for detection of FRET using TIRF-FLIM imaging. We have also generated the first data from the application of TIRF-FLIM imaging to FRET detection within nAChRs. If the described challenges to this new technique are met, TIRF-FLIM-FRET may be a promising method for differentiation of nAChR receptor stoichiometry. It remains to be seen if the constraints of the biological system allow determination of donor position within the receptor pentamer using this technique.

## *Chapter 6*

### *Conclusions*

Nicotinic acetylcholine receptors (nAChRs) are widespread throughout the body in both the peripheral and central nervous systems. In the brain, nAChRs are ubiquitously expressed. However, layers of regulation are involved in the highly specific localization of these important receptors [3]. Individual brain regions may express only certain subtypes of the receptors, and this expression may even be sub-region specific. For instance,  $\alpha 4\beta 2$  receptors are expressed in many regions of the brain, including the pre-frontal cortex (PFC). However,  $\alpha 5\alpha 4\beta 2$  receptors are highly concentrated only in cortical layer VI [7, 10]. Furthermore, cell types within sub-region offer an additional layer of regional specificity. In the mid-brain ventral tegmental area (VTA) glutamatergic neurons express  $\alpha 7$  receptors, GABA neurons are known to express  $\alpha 4\beta 2$  and  $\alpha 6^*$  receptors on dopaminergic neurons in the same region are important for dopamine release [59, 61].

Receptor composition and stoichiometry confers unique biophysical and pharmacological properties to each receptor sub-type. This variation in receptor function influences which brain regions are active in response to agonists, the concentrations at which certain cell-types are activated, and the nature of that activation. Accessory subunits such as  $\alpha 5$  and  $\beta 3$  act as modulators to amplify or attenuate a chemical signal either by changing agonist affinity or increasing ionic permeability, and  $\beta$  subunits can affect surface occupancy of receptors on the plasma membrane [13, 23, 56]. Stoichiometry is the key to many of the diverse effects of nAChR activation. Preferential upregulation of  $(\alpha 4)_2(\beta 2)_3$  stoichiometry receptors after nicotine exposure may contribute to the development of

nicotine tolerance and the development of disease states such as autosomal dominant nocturnal frontal lobe epilepsy (ADNFLE) [1, 6, 36].

Determination of nAChR composition and stoichiometry is a challenging one. Many receptor subtypes have been identified, and the regions of their distribution elucidated; however, the number of specific subunits within a nAChR is not always known.

Additionally, isolation of specific receptor populations for individual study is difficult, especially if unique agonists or antagonists do not exist, as in the case of the accessory subunits [13]. Recently, direct visualization of receptor composition has become possible using fluorescent microscopy techniques. Creation of fluorescently labeled nAChR subunits by fusion with fluorescent protein variants (FPs) has provided exciting alternatives to electrophysiology for the study of selective pharmacological effects on nAChR number, stoichiometry, and subcellular behavior [36]. Additionally, the ability to visualize nascent nAChRs, still in intracellular compartments, yields an advantage over immunohistochemistry, which require cell permeabilization, or electrophysiological assays that are restricted to measuring function of mature receptors. Advanced imaging techniques have been applied to fluorescent nAChRs including confocal and TIRF microscopy, FRET measurements, single molecule visualization, and FLIM. Combined, these methods form a powerful tool box for elucidation of intracellular assembly, processing, and trafficking of nAChRs [6, 21-23, 26, 46]. However, these methods are not without their own limitations.

The data presented in this thesis make a strong case for systematic optimization of the methods for studying fluorescent nAChRs and suggest that caution must be taken when interpreting fluorescence data. The placement of FP labels within the M3-M4 loop of the nAChR is crucial to satisfy the distance requirements of FRET and avoids steric

interference with ligand binding domains, which may be important for interactions with agonists or molecular chaperones, but the M3-M4 loop also contains sequencing motifs important for assembly of the nAChR pentamer and interaction with vesicular trafficking machinery [23, 35]. Chapter 3 has demonstrated that perturbation of the  $\alpha 5$  M3-M4 region with a large fluorescent protein  $\geq 4$  times the size of the loop itself may make wild-type behavior impossible for such an encumbered subunit. Less invasive labeling methods to ensure wild-type behavior of receptors and their subunits are available but few utilize completely non-invasive methods. Site specific incorporation of fluorescent unnatural amino acids (UAAs) would be ideal for such a purpose. UAAs have been used in preliminary experiments, but use of these systems is tricky, and the technique has not been sufficiently compatible for expression in mammalian cells [62-63].

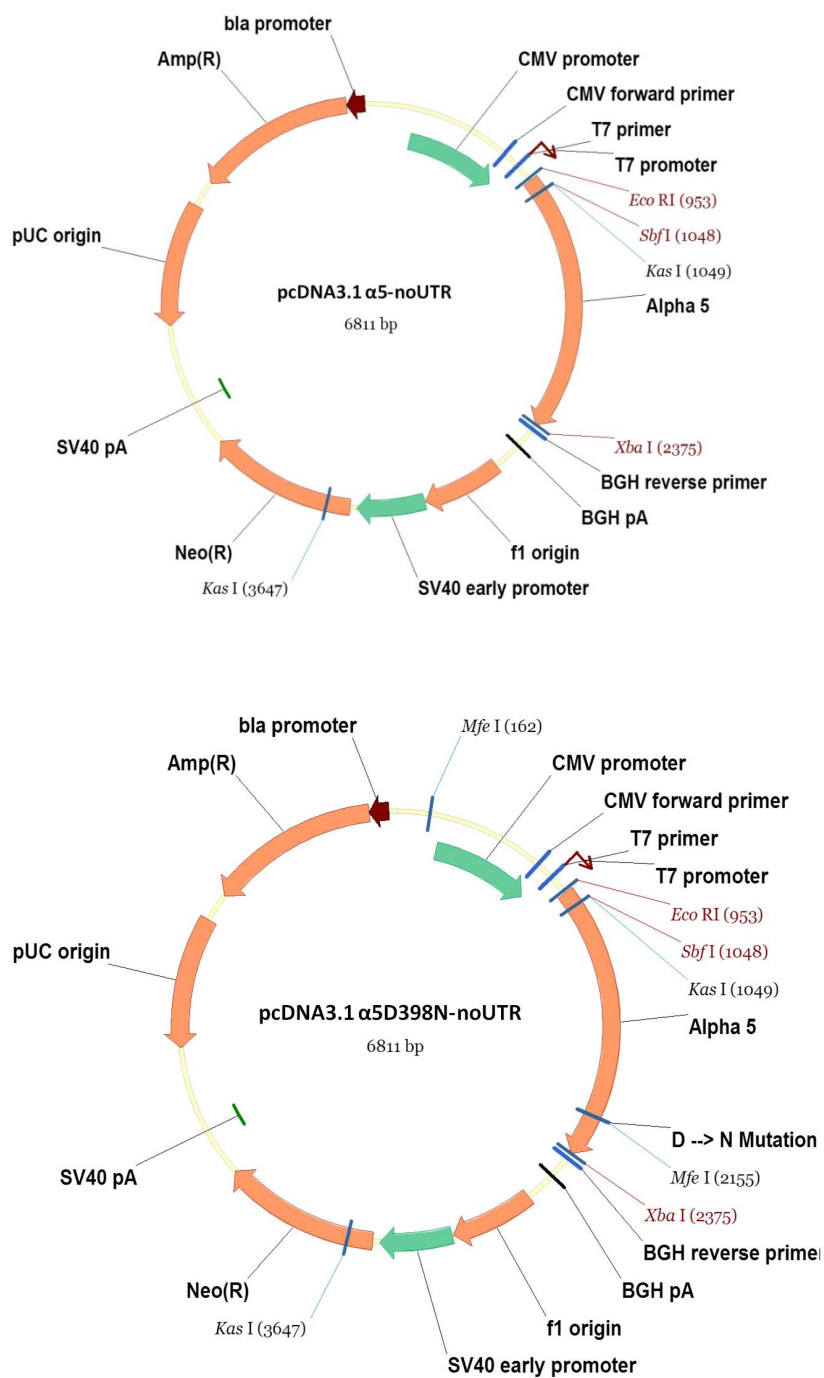
NFRET analysis has been proposed in the literature as a technique for elucidation of nAChR stoichiometries. However, findings presented in chapter 4 of this thesis suggest that these results may have been over interpreted. While it is likely that intracellular changes in pre-receptor assemblies are detectable after exposure to drugs such as nicotine or dihydro- $\beta$ -erythroidine, these changes may not directly correlate to differences in stoichiometry at the plasma membrane. The statistical similarity of NFRET histograms generated from cell populations with and without the ability to form mature receptor complexes is not encouraging. Further experiments could be performed to examine changes to NFRET% in the same population of cells after drug exposure to determine whether any meaningful conclusions about receptor stoichiometry can be drawn from NFRET histograms, but it remains a reliable measure of intracellular interaction of fluorescent nAChR subunits.

The combination of TIRF and FLIM techniques offers a unique opportunity for high resolution detection of FRET interactions in a selective population of mature nAChRs. It is possible that further optimization of the fluorescent nAChR constructs used in the experiments presented in chapter 5 will allow rigorous characterization of  $E_{\text{FRET}}$  values for individual geometric relationships within the nAChR pentamer. Once standard measurements are performed for the mouse muscle nAChR, the same FRET relationships can be applied to measurements of neuronal nAChR pentamers of unknown stoichiometric composition. If the trafficking restrictions can be overcome, TIRF-FLIM-FRET (or single molecule photo-bleaching as performed by Richards et al.) remains the most direct method for stoichiometric determination of nAChRs.

Without exact knowledge of nAChR composition and stoichiometry, design of unique pharmacological agents for selective activation or inactivation of many receptor sub-types is unlikely. nAChRs are notoriously hard to crystallize due to their multi-transmembrane nature and many subunits. This lack of detailed structural information contributes to a disparity of effective pharmaceuticals for the treatment of nAChR related diseases and nicotine addiction [64-65]. Understanding subtle differences in distributions of receptor composition and stoichiometry will move us closer to a more complete picture of the molecular mechanisms underlying nAChR interactions within networks of neuronal function, disease, and addiction. Judicious application of fluorescent microscopy techniques will certainly be an important tool in elucidation of these mechanisms. The data presented here represents one small step towards this understanding.

## Appendix i

### Plasmid Maps of pcDNA3.1(+) $\alpha$ 5-no UTR and pcDNA3.1(+) $\alpha$ 5D398N-no UTR



*PCR Protocol for extension of Chrna5*

PCR Mix:

	<b>reagent</b>	<b>μL</b>
alpha5	template	0.5
	quick solution	3
	10x buffer	5
	Forward primer 50μM	1
	Reverse primer 50μM	1
	dNTPs	1
	Pfu turbo hotstart polymerase	1.5
	dH2O	37
<hr/>		
	Total Volume	50

PCR Cycle Protocol

Quick change reaction Conditions:

<b>Temp</b>	<b>Time</b>
95°C	4min
95°C	30sec
60°C	2min
68°C	16min
68°C	10min
4°C	∞

Extension of *Chrna5* gene

<b>Temp</b>	<b>Time</b>
95°C	4min
95°C	30sec
52°C	2min
68°C	16min
68°C	10min
4°C	∞

## **Appendix ii**

### *Transfection protocols*

#### **Transfection: N2a Cells for Fluorescence Imaging**

90,000 cells plated on 3 in Matek imaging dishes 24 h before transfection

heat Expressfect lippofection reagent @ 50°C to bring into solution

pipette DNA into 100uL DMEM/dish

pipette 4uL expressfect into 100uL DMEM/ transfection

add 100uL expressfect/DMEM mix to DNA

Incubate 20 min at 25°C

Remove all but 1mL cell media from dish and add all 200uL of

transfection mixture.

Incubate 4 h at 37°C

Rinse dishes with 1mL media

Replace 3 mL fresh media

incubate ~48 h before imaging

#### **Imaging sample preparation: N2a Cells**

20min before imaging, heat objective oil and Leibovitz media to 37°C

image cells in 2mL Leibovitz media

**N2a Transfection and Differentiation Protocol**  
**Also Transfection Protocol for HEK 293-T cells (miRNA experiments)**

On a 3 inch diameter Matek cell culture dish, plate cells ~ 60,000cells/dish in antibiotic free media 24 h before transfection

Remove cell media from wells, add 2 mL Opti-mem

Prepare DNA

250uL Opti-mem/well/tube

0.5ug DNA/subunit/well

Prepare Lipofectamine2000

250uL Opti-mem/well/tube

2uL Lipo/well

incubate 5min

DNA+Lipofectamine2000 Mix:

Add Lipo2000+Opti-mem solution to DNA+Opti-mem in 1tube:1tube manner

(total volume/tube approx 500uL)

Incubate 20min to allow complex to form

DNA+Lipofectamine2000+Cells

Add full 500uL volume of DNA+Lipo mixture to wells in a 1:tube:1well/dish manner

Incubate 24h then image/assay

**Transfection of Primary Neuronal Cultures in 3 inch Imaging Dishes Using Lipofectamine2000: \*Non-optimized\***

- 1) In a 15 mL conical tube, combine 100 uL Optimem + 4 uL Lipo2000 / dish and incubate 5 min in the hood
- 2) In an eppendorf tube combine 100 uL Optimem + DNA, repeat per number of dishes to be transfected
- 3) Add 100 uL Optimem Lipo2000 soln. to each ependorf and incubate for 25 min
- 4) Remove 1.2 mL media from each culture dish and store in a 24 well plate in the incubator
- 5) Add the Lipo2000+DNA in Optimem mixture to the culture dishes in 1:1 manner
- 6) Incubate for 4 h
- 7) Rinse dishes with warm growth media to remove transfection complex
- 8) Replace media with 1.2 mL conditioned media and 1 mL new warm growth media

**Transfection of Primary Neuronal Cultures in 3 in Imaging Dishes Using Lipofectamine2000 + Optimem:\*Optimized\***

- 1) In a 15 mL conical tube, combine 100 uL Optimem + 4 uL Lipo2000 / dish and incubate 5 min in the hood
- 2) In an ependorf tube combine 100 uL Optimem + DNA, repeat per number of dishes to be transfected
- 3) Add 100 uL Optimem Lipo2000 soln. to each ependorf and incubate for 25 min
- 4) Remove 1.0 mL media from each culture dish and store in a 24 well plate in the incubator
- 5) Remove 0.5 mL and discard
- 6) Replace 0.5 mL with 0.5 mL warm Optimem
- 7) Add the Lipo2000+DNA in mixture from step 3) to the culture dishes
- 8) Incubate for 4 h
- 9) Remove media from dish, leaving a small bubble of liquid over the round cover slip
- 10) Replace media with 1 mL conditioned media and 1 mL new warm growth media

### *Maintenance of Neuronal Culture*

#### **Recipe for Neuronal Growth Media:**

500 mL Neurobasal Media

10 mL B27 supplement (freezer)

1.25 mL Glutamax (freezer)

#### **Poly(D) Lysine Coating For Imaging Dishes:**

- 1) Dilute 1 mL of 1% stock aliquot of Poly(D)-L to a total volume of 10 mL with DI water
- 2) Pipette 200uL 0.1% Poly(D)-L onto the glass cover slip within the imaging dish.  
(250uL for 14mm cover slip dishes)
- 3) Incubate dish with Poly(D)-L in the incubator for 1 h
- 4) Aspirate the remaining Poly(D)-L
- 5) Wash with DI water 2 X 2mL
- 6) Let dishes dry in the hood for 30 – 60 min
- 7) Dishes are ready for neurons to be plated

#### **Plating Mouse Neurons on 3 in Imaging Dishes from Mouse Prep: makes 20 dishes**

- 1) To make plating media, combine 48.5 mL neuronal growth media + 1.5 mL Equine Serum (ES)
- 2) Sheri leaves the neurons in a tube in TC fridge  
Note: remember to use the large tips for the p-1000 pipette when pipetting neurons!
- 3) ~60,000 neurons plated per dish \* 20 dishes = 1,200,000 total cell needed.  
 $1.2 * 10^6$  cells / concentration of sheri's prep = volume to dilute (usually between 150 -200uL)

- 4) Dilute the  $1.2 \times 10^6$  cells to a volume of 4 mL with the plating media
- 5) Plate 200uL of this dilution on to each imaging dish (pre coated with Poly(D)-L)  
Store the remaining plating media in the 37 deg water bath
- 6) Incubate the dishes in the incubator for 30 min so that the neurons will sit down on the dish
- 7) Add 2 mL warm plating media to each dish
- 8) Return dishes to the incubator for 3 days

**Ara-C Treatment of Primary Neuronal Culture: makes 20 dishes**

- 1) Thaw Ara-C (stock concentration is 100 uM) and warm 20 mL growth media in 37 deg bath
- 2) Add 40 uL Ara-C to 20 mL neuronal growth media for a total concentration of 2 uM Ara-C
- 3) Remove 1 mL of media from each culture dish and replace with 1 mL of 2 uM Ara-C soln.
- 4) Return dishes to the incubator
- 5) 24 h after addition of Ara-C, perform a  $\frac{1}{2}$  media change with fresh, warm, growth media

### *Imaging Settings*

#### **Live imaging conditions for clonal cell lines expressing fluorescent nAChRs:**

Eclipse C1si laser-scanning confocal microscope with a 63x 1.4 NA Plan Apo oil immersion lens.

60  $\mu$ M pinhole

Pixel dwell time 6.72  $\mu$ s

Spectral Gain 200

Cells were excited with either 488 nm or 561 nm laser at (2.5% - 35% power)

Images were collected in 512 X 512 pixel format. Single images were taken as an average of 3 scans.

#### **Live imaging conditions for cortical neurons expressing fluorescent nAChRs:**

Eclipse C1si laser-scanning confocal microscope with a 60x Plan Apo oil immersion lens.

60  $\mu$ M pinhole

Pixel dwell time 6.72  $\mu$ s

Spectral Gain 200

Cells were excited with either 488 nm or 561 nm laser at (15% - 35% power)

Images were collected in 512 X 512 pixel format.

Single images were taken as an average of 3 scans.

Z-stack images were collected as stacks of 1  $\mu$ m step images from the top of the cell to the coverslip.

## Appendix iii

### *Image workup for NFRET experiments*

Nikon EZ-Ci software was used for spectral unmixing

Unmixing Imaging files:

1<sup>st</sup> Unmix the Acceptor (mCherry) Files

2<sup>nd</sup> Unmix the Donor (mEGFP) Files

How to make SBT montage and profiles: . . .

Donor model (GFP only)

1. Open all GFP unmixed, 1<sup>st</sup> window is “cherry channel”
2. Make stack
3. Make montage of stack
4. Label “donor model, FRET montage” (scale factor 1)

1. Open all GFP unmixed, 2<sup>nd</sup> window is “donor channel”
2. Make stack
3. Make montage
4. Label “donor model, donor montage” (scale factor 1)
5. Open FRET montage, open donor montage
6. Make stack of montages
7. Open pix fret etc.

Acceptor model (cherry only)

1. Open GFP unmixed, 1<sup>st</sup> window is “FRET channel”
2. Make stack
3. Make montage
4. Label “acceptor model FRET montage”

1. Open Cherry unmixed, 1<sup>st</sup> window is “acceptor channel”
2. Make stack
3. Make montage
4. Label “acceptor model, acceptor montage”

Open FRET montage, open acceptor montage

Make stack of montages

Open PixFRET

To analyze a cell

Open GFP unmixed

Open mCherry unmixed (close 2<sup>nd</sup> window)

Select ROI

Calculate FRET

Calculate NFRET

Save histogram as .xls

ALWAYS DUPLICATE DATA BEFORE PROCESSING

Matlab Script:

```
saveBinRepeatsbigtxt('C:(FILE NAME OF SAVED NFRET XLS FILES)l.xls', '-all', '-  
exclude', 0);
```

Confocal Scale Bars in ImageJ 60X objective:

1 pixel = 0.207 microns

TIRF For Scale Bars in ImageJ 100X 1.45NA objective:

1pixel = 0.16 microns

**Total FRETing Pixels t-test  $\alpha_4$  vs  $\alpha_4\beta_2$** 

Normality Test (Shapiro-Wilk)

Dataset	N	W	P Value	Decision
DATA1_a4ga4c	25	0.76789	0.00003	Not Normal at 0.05 level

[4/4/2011 15:31 "/Data1" (2455655)]

Normality Test (Shapiro-Wilk)

Dataset	N	W	P Value	Decision
DATA2_a4ga4c b2	22	0.83854	0.00155	Not Normal at 0.05 level

[4/4/2011 15:31 "/Data1" (2455655)]

Two Sample Independent t-Test

Summary Statistics

Sample	N	Mean	SD
1. Data1_a4ga4c	25	14623.2	17207.40465
2. Data2_a4ga4c b2	22	14601.5	13431.16611

Difference of Means: 21.7

Null Hypothesis: Mean1 - Mean2 &gt;= 0

Alternative Hypothesis: Mean1 - Mean2 &lt; 0

t	DoF	P Value
0.00477	45	0.50189

At the 0.05 level, the difference of the population means is not significantly less than the test difference (0).

**Total FRETing Pixels t-test  $\alpha 5\alpha 4$  vs  $\alpha 5\alpha 4\beta 2$** 

Normality Test (Shapiro-Wilk)

Dataset	N	W	P Value	Decision
DATA1_a5ga4c	13	0.83437	0.01680	Not Normal at 0.05 level

[4/4/2011 15:26 "/Data1" (2455655)]

Normality Test (Shapiro-Wilk)

Dataset	N	W	P Value	Decision
DATA2_a5ga4c b2	23	0.78307	0.00011	Not Normal at 0.05 level

[4/4/2011 15:26 "/Data1" (2455655)]

Two Sample Independent t-Test

Summary Statistics

Sample	N	Mean	SD
1. Data1_a5ga4c	13	11327.38462	10944.81719
2. Data2_a5ga4c b2	23	7330.6087	6799.63318

Difference of Means: 3996.77592

Null Hypothesis: Mean1 - Mean2  $\geq$  0Alternative Hypothesis: Mean1 - Mean2  $<$  0

t	DoF	P Value
1.35563	34	0.90792

At the 0.05 level, the difference of the population means is not significantly less than the test difference (0).

**Mean Cell Values t-test  $\alpha_5\alpha_4$  vs  $\alpha_5\alpha_4\beta_2$** 

Normality Test (Shapiro-Wilk)

Dataset	N	W	P Value
Decision			
-----			
DATA1_a5ga4c	13	0.90306	0.14342
Normal at 0.05 level			

[4/4/2011 15:20 "/Data1" (2455655)]

Normality Test (Shapiro-Wilk)

Dataset	N	W	P Value
Decision			
-----			
DATA1_a5ga4c b2	23	0.94752	0.26205
Normal at 0.05 level			

[4/4/2011 15:21 "/Data1" (2455655)]

Two Sample Independent t-Test

Summary Statistics

Sample	N	Mean	SD
SE			
-----			
1. Data1_a5ga4c	13	6.62979	1.47155
0.40814			
2. Data2_a5ga4c b2	23	6.81496	1.37013
0.28569			

Difference of Means: -0.18517

Null Hypothesis: Mean1 - Mean2 &gt;= 0

Alternative Hypothesis: Mean1 - Mean2 &lt; 0

t	DoF	P Value
-----		
-0.37934	34	0.35340
-----		

At the 0.05 level, the difference of the population means is not significantly less than the test difference (0).

## Bibliography

1. Brodtkorb, E. and F. Picard, *Tobacco habits modulate autosomal dominant nocturnal frontal lobe epilepsy*. *Epilepsy & Behavior*, 2006. **9**(3): p. 515-520.
2. Unwin, N., *Refined Structure of the Nicotinic Acetylcholine Receptor at 4Å Resolution*. *Journal of Molecular Biology*, 2005. **346**(4): p. 967-989.
3. Albuquerque, E.X., et al., *Mammalian Nicotinic Acetylcholine Receptors: From Structure to Function*. *Physiological Reviews*, 2009. **89**(1): p. 73-120.
4. Nelson, M.E., et al., *Alternate Stoichiometries of alpha4beta2 Nicotinic Acetylcholine Receptors*. *Molecular Pharmacology*, 2003. **63**(2): p. 332-341.
5. Zwart, R. and H.P.M. Vijverberg, *Four Pharmacologically Distinct Subtypes of alpha4beta2 Nicotinic Acetylcholine Receptor Expressed in Xenopus laevis Oocytes*. *Molecular Pharmacology*, 1998. **54**(6): p. 1124-1131.
6. Son, C.D., et al., *Nicotine Normalizes Intracellular Subunit Stoichiometry of Nicotinic Receptors Carrying Mutations Linked to Autosomal Dominant Nocturnal Frontal Lobe Epilepsy*. *Molecular Pharmacology*, 2009. **75**(5): p. 1137-1148.
7. Gotti, C., M. Zoli, and F. Clementi, *Brain nicotinic acetylcholine receptors: native subtypes and their relevance*. *Trends in Pharmacological Sciences*, 2006. **27**(9): p. 482-491.
8. Fowler, C.D., et al., *Habenular alpha5 nicotinic receptor subunit signalling controls nicotine intake*. *Nature*, 2011. **471**(7340): p. 597-601.
9. Mao, D., et al., *The alpha4beta2alpha5 nicotinic cholinergic receptor in rat brain is resistant to up-regulation by nicotine in vivo*. *Journal of Neurochemistry*, 2008. **104**(2): p. 446-456.
10. Bailey, C.D.C., et al., *The Nicotinic Acetylcholine Receptor alpha5 Subunit Plays a Key Role in Attention Circuitry and Accuracy*. *The Journal of Neuroscience*, 2010. **30**(27): p. 9241-9252.
11. Salminen, O., et al., *Subunit Composition and Pharmacology of Two Classes of Striatal Presynaptic Nicotinic Acetylcholine Receptors Mediating Dopamine Release in Mice*. *Molecular Pharmacology*, 2004. **65**(6): p. 1526-1535.
12. Kuryatov, A., et al., *Nicotine Acts as a Pharmacological Chaperone to Up-Regulate Human alpha4beta2 Acetylcholine Receptors*. *Molecular Pharmacology*, 2005. **68**(6): p. 1839-1851.
13. Kuryatov, A., J. Onksen, and J. Lindstrom, *Roles of Accessory Subunits in alpha4beta2\* Nicotinic Receptors*. *Molecular Pharmacology*, 2008. **74**(1): p. 132-143.
14. Tapia, L., A. Kuryatov, and J. Lindstrom, *Ca<sup>2+</sup> Permeability of the (alpha4)<sub>3</sub>(beta2)<sub>2</sub> Stoichiometry Greatly Exceeds That of (alpha4)<sub>2</sub>(beta2)<sub>3</sub> Human Acetylcholine Receptors*. *Molecular Pharmacology*, 2007. **71**(3): p. 769-776.
15. Gorbounova, O., et al., *Chronic Ethanol Treatment Decreases [3H]Epibatidine and [3H]Nicotine Binding and Differentially Regulates mRNA Levels of Nicotinic Acetylcholine Receptor Subunits Expressed in M10 and SH-SY5Y Neuroblastoma Cells*. *Journal of Neurochemistry*, 1998. **70**(3): p. 1134-1142.
16. Young, R.P., et al., *Lung cancer gene associated with COPD: triple whammy or possible confounding effect?* *European Respiratory Journal*, 2008. **32**(5): p. 1158-1164.
17. Hung, R.J., et al., *A susceptibility locus for lung cancer maps to nicotinic acetylcholine receptor subunit genes on 15q25*. *Nature*, 2008. **452**(7187): p. 633-637.
18. Bierut, L.J., et al., *Variants in nicotinic receptors and risk for nicotine dependence*. *American Journal of Psychiatry*, 2008. **165**(9): p. 1163-71.
19. Ramirez-Latorre, J., et al., *Functional contributions of [alpha]5 subunit to neuronal acetylcholine receptor channels*. *Nature*, 1996. **380**(6572): p. 347-351.

20. Marotta, C.B., et al., *Probing the non-canonical interface for agonist interaction with an alpha5 containing nicotinic acetylcholine receptor*. *Neuropharmacology*, 2014 (0).
21. Nashmi, R., et al., *Assembly of alpha4beta2 Nicotinic Acetylcholine Receptors Assessed with Functional Fluorescently Labeled Subunits: Effects of Localization, Trafficking, and Nicotine-Induced Upregulation in Clonal Mammalian Cells and in Cultured Midbrain Neurons*. *The Journal of Neuroscience*, 2003. **23**(37): p. 11554-11567.
22. Drenan, R.M., et al., *Subcellular Trafficking, Pentameric Assembly, and Subunit Stoichiometry of Neuronal Nicotinic Acetylcholine Receptors Containing Fluorescently Labeled alpha6 and beta3 Subunits*. *Molecular Pharmacology*, 2008. **73**(1): p. 27-41.
23. Srinivasan, R., et al., *Nicotine up-regulates alpha4beta2 nicotinic receptors and ER exit sites via stoichiometry-dependent chaperoning*. *The Journal of General Physiology*, 2011. **137**(1): p. 59-79.
24. Zhang, G., V. Gurtu, and S.R. Kain, *An Enhanced Green Fluorescent Protein Allows Sensitive Detection of Gene Transfer in Mammalian Cells*. *Biochemical and Biophysical Research Communications*, 1996. **227**(3): p. 707-711.
25. Zacharias, D.A., et al., *Partitioning of Lipid-Modified Monomeric GFPs into Membrane Microdomains of Live Cells*. *Science*, 2002. **296**(5569): p. 913-916.
26. Srinivasan, R., et al., *Pharmacological Chaperoning of Nicotinic Acetylcholine Receptors Reduces the Endoplasmic Reticulum Stress Response*. *Molecular Pharmacology*, 2012. **81**(6): p. 759-769.
27. Dash, B., Y. Chang, and R.J. Lukas, *Reporter Mutation Studies Show That Nicotinic Acetylcholine Receptor (nAChR)  $\alpha$ 5 Subunits and/or Variants Modulate Function of alpha6\*-nAChR*. *Journal of Biological Chemistry*, 2011. **286**(44): p. 37905-37918.
28. Groot-Kormelink, P.J., J.P. Boorman, and L.G. Sivilotti, *Formation of functional alpha3beta4alpha5 human neuronal nicotinic receptors in Xenopus oocytes: a reporter mutation approach*. *British Journal of Pharmacology*, 2001. **134**(4): p. 789-796.
29. Labarca, C., et al., *Channel gating governed symmetrically by conserved leucine residues in the M2 domain of nicotinic receptors*. *Nature*, 1995. **376**(6540): p. 514-516.
30. Kosik, K.S., *The neuronal microRNA system*. *Nat Rev Neurosci*, 2006. **7**(12): p. 911-920.
31. Simon, D.J., et al., *The MicroRNA miR-1 Regulates a MEF-2-Dependent Retrograde Signal at Neuromuscular Junctions*. *Cell*, 2008. **133**(5): p. 903-915.
32. Bailey, C.D.C., et al., *Nicotinic alpha5 Subunits Drive Developmental Changes in the Activation and Morphology of Prefrontal Cortex Layer VI Neurons*. *Biological Psychiatry*, 2012. **71**(2): p. 120-128.
33. Berardi, N., T. Pizzorusso, and L. Maffei, *Critical periods during sensory development*. *Current Opinion in Neurobiology*, 2000. **10**(1): p. 138-145.
34. Winzer-Serhan, U.H. and F.M. Leslie, *Expression of alpha5 nicotinic acetylcholine receptor subunit mRNA during hippocampal and cortical development*. *The Journal of Comparative Neurology*, 2005. **481**(1): p. 19-30.
35. Kracun, S., et al., *Influence of the M3-M4 intracellular domain upon nicotinic acetylcholine receptor assembly, targeting and function*. *British Journal of Pharmacology*, 2008. **153**(7): p. 1474-1484.
36. Lester, H.A., Xiao, C., Srinivasan, R., Son, C.D., Miwa, J., Pantoja, R., Banghart, M.R., Dougherty, D.A., Goate, A.M., and Wang, J.C., *Nicotine is a Selective Pharmacological Chaperone of Acetylcholine Receptor Number and Stoichiometry. Implications for Drug Discovery*. *The AAPS Journal*, 2009. **11**(1): p. 167-177.

37. Michelsen, K., H. Yuan, and B. Schwappach, *Hide and run: Arginine-based endoplasmic-reticulum-sorting motifs in the assembly of heteromultimeric membrane proteins*. EMBO Rep, 2005. **6**(8): p. 717-722.
38. Mancias, J.D. and J. Goldberg, *Structural basis of cargo membrane protein discrimination by the human COPII coat machinery*. EMBO J, 2008. **27**(21): p. 2918-2928.
39. Wang, Y., et al., *Mouse RIC-3, an Endoplasmic Reticulum Chaperone, Promotes Assembly of the alpha7 Acetylcholine Receptor through a Cytoplasmic Coiled-Coil Domain*. The Journal of Neuroscience, 2009. **29**(40): p. 12625-12635.
40. Lakowicz, J.R., *Principles of Fluorescence Spectroscopy*. 3 ed. 2006, New York: Springer.
41. Truong, K. and M. Ikura, *The use of FRET imaging microscopy to detect protein-protein interactions and protein conformational changes in vivo*. Current Opinion in Structural Biology, 2001. **11**(5): p. 573-578.
42. Kenworthy, A.K., *Imaging Protein-Protein Interactions Using Fluorescence Resonance Energy Transfer Microscopy*. Methods, 2001. **24**(3): p. 289-296.
43. Zheng, J., *FRET and Its Biological Application as a Molecular Ruler*, in *Biomedical Applications of Biophysics*, T. Jue, Editor. 2010, Humana Press. p. 119-136.
44. Marvin, J.S., Borghuis, B.G., Tian, L., Cichon, J., Harnett, M.T., Akerboom, J., Gordus, A., Renninger, S.L., Chen, T.W., Bargmann, C.I., Orger, M.B., Schreiter, E.R., Demb, J.B., Gan, W.B., Hires, S.A., and Looger, L.L., *An optimized fluorescent probe for visualizing glutamate neurotransmission*. Nature Methods, 2013. **10**(2): p. 162 - 170.
45. Brustad, E.M., et al., *A General and Efficient Method for the Site-Specific Dual-Labeling of Proteins for Single Molecule Fluorescence Resonance Energy Transfer*. Journal of the American Chemical Society, 2008. **130**(52): p. 17664-17665.
46. Srinivasan, R., et al., *Förster Resonance Energy Transfer (FRET) Correlates of Altered Subunit Stoichiometry in Cys-Loop Receptors, Exemplified by Nicotinic alpha4beta2*. International Journal of Molecular Sciences, 2012. **13**(8): p. 10022-10040.
47. Feige, J.N., et al., *PixFRET, an ImageJ plug-in for FRET calculation that can accommodate variations in spectral bleed-throughs*. Microscopy Research and Technique, 2005. **68**(1): p. 51-58.
48. Wu, J. and R.J. Lukas, *Naturally-expressed nicotinic acetylcholine receptor subtypes*. Biochemical Pharmacology, 2011. **82**(8): p. 800-807.
49. Gotti, C., et al., *Expression of Nigrostriatal alpha6-Containing Nicotinic Acetylcholine Receptors Is Selectively Reduced, but Not Eliminated, by beta3 Subunit Gene Deletion*. Molecular Pharmacology, 2005. **67**(6): p. 2007-2015.
50. Richards, C.I., Srinivasan, R., Xiao, C., Mackey, E.D.W., Miwa, J.M. and Lester, H., *Trafficking of alpha4\* nicotinic receptors revealed by superecliptic phlorin*. Journal of Biological Chemistry, 2011. **286**(36): p. 31241 - 31249.
51. Wallrabe, H. and A. Periasamy, *Imaging protein molecules using FRET and FLIM microscopy*. Current Opinion in Biotechnology, 2005. **16**(1): p. 19-27.
52. Becker, W., et al., *Fluorescence lifetime imaging by time-correlated single-photon counting*. Microscopy Research and Technique, 2004. **63**(1): p. 58-66.
53. Lakowicz, J.R., et al., *Fluorescence lifetime imaging*. Analytical Biochemistry, 1992. **202**(2): p. 316-330.
54. Axelrod, D., *Cell-substrate contacts illuminated by total internal reflection fluorescence*. The Journal of Cell Biology, 1981. **89**(1): p. 141-145.
55. Kalamida, D., et al., *Muscle and neuronal nicotinic acetylcholine receptors*. FEBS Journal, 2007. **274**(15): p. 3799-3845.

56. Papke, R.L., L. Wecker, and J.A. Stitzel, *Activation and Inhibition of Mouse Muscle and Neuronal Nicotinic Acetylcholine Receptors Expressed in Xenopus Oocytes*. Journal of Pharmacology and Experimental Therapeutics, 2010. **333**(2): p. 501-518.
57. Seeds, N.W., et al., *Regulation of Axon Formation by Clonal Lines of a Neural Tumor*. Proceedings of the National Academy of Sciences, 1970. **66**(1): p. 160-167.
58. Ganesan, S., et al., *A dark yellow fluorescent protein (YFP)-based Resonance Energy-Accepting Chromoprotein (REACb) for Förster resonance energy transfer with GFP*. Proceedings of the National Academy of Sciences of the United States of America, 2006. **103**(11): p. 4089-4094.
59. Wu, B., Y. Chen, and J.D. Müller, *Fluorescence Fluctuation Spectroscopy of mCherry in Living Cells*. Biophysical Journal, 2009. **96**(6): p. 2391-2404.
60. Galperin, E., V.V. Verkhusha, and A. Sorkin, *Three-chromophore FRET microscopy to analyze multiprotein interactions in living cells*. Nat Meth, 2004. **1**(3): p. 209-217.
61. Drenan, R.M., et al., *In Vivo Activation of Midbrain Dopamine Neurons via Sensitized, High-Affinity  $\alpha 6^*$  Nicotinic Acetylcholine Receptors*. Neuron, 2008. **60**(1): p. 123-136.
62. Pantoja, R., et al., *Single-Molecule Imaging of a Fluorescent Unnatural Amino Acid Incorporated Into Nicotinic Receptors*. Biophysical Journal, 2009. **96**(1): p. 226-237.
63. Shen, B., et al., *Genetically Encoding Unnatural Amino Acids in Neural Stem Cells and Optically Reporting Voltage-Sensitive Domain Changes in Differentiated Neurons*. STEM CELLS, 2011. **29**(8): p. 1231-1240.
64. Henningfield, J.E., *Nicotine Medications for Smoking Cessation*. New England Journal of Medicine, 1995. **333**(18): p. 1196-1203.
65. Gonzales, D., et al., *Varenicline, an  $\alpha 4\beta 2$  nicotinic acetylcholine receptor partial agonist, vs sustained-release bupropion and placebo for smoking cessation: A randomized controlled trial*. Journal of the American Medical Association, 2006. **296**(1): p. 47-55.